PHILOSOPHICAL TRANSACTIONS OF THE ROYAL SOCIETY A MATHEMATICAL, PHYSICAL & ENGINEERING SCIENCES

Vibration of an Elastic Strip with Varying Curvature

J. F. M. Scott and J. Woodhouse

Phil. Trans. R. Soc. Lond. A 1992 **339**, 587-625
doi: 10.1098/rsta.1992.0052

Vibration of an elastic strip with varying curvature

By J. F. M. Scott[1] and J. Woodhouse[2]

[1] *Topexpress Ltd, Poseidon House, Castle Park, Cambridge CB3 0RD, U.K.*

[2] *Cambridge University Engineering Department, Trumpington Street, Cambridge CB2 1PZ, U.K.*

Contents

The vibrational behaviour of an elastic strip with varying curvature is investigated. The case of vibration which is predominantly transverse is considered, and it is shown that when the strip is S-shaped, certain of the normal modes may be confined to the vicinity of the inflection point of the S by a process of total internal reflection from points where the curvature reaches critical values. This confinement can produce modes with extraordinarily low damping factors. Asymptotic analysis is compared with experimental measurements on a strip in several S-shaped configurations, and very good agreement is demonstrated for modal frequencies and shapes. Mathematically, the lower modes turn out to be analogous to those of the one-dimensional harmonic oscillator in quantum mechanics.

This mode confinement behaviour occurs for all waveguide branches except the lowest, 'bending beam', branch. In this particular case, wave propagation is insensitive to curvature. However, an interesting phenomenon associated with curvature is found: the successive mode shapes do not display the normal alternation of symmetry and antisymmetry with respect to the centre of the strip. The effect is shown to result from the constraint on axial movement produced by fixed end conditions. For the geometry of the experiments, this constraint raises the frequencies of antisymmetric modes in a characteristic way while leaving the

Phil. Trans. R. Soc. Lond. A (1992) **339**, 587–625
Printed in Great Britain

symmetric modes unaltered, thus changing the mode sequence. Theory is developed which gives reasonable quantitative agreement with the observations.

1. Introduction and formulation

The origin of this study lies in the behaviour of the 'musical saw'. When an ordinary hand-saw is bent into an S-shape, an interesting acoustical effect can occur. Tapping the blade of the saw reveals that beyond a certain critical degree of curvature, a very lightly damped vibration mode appears, confined in the vicinity of the point of inflection on the S. Even though the saw blade is held in the hands, the damping of this mode is so low as to be comparable with the intrinsic internal damping of the steel of which the blade is made. This confined mode of vibration can be excited with a violin bow, and the resulting wailing sound is what is usually described as the 'musical saw'. Our concern here is not with this continuous excitation, however, but with the mechanism of confinement and the nature of the modes of vibration. The confinement phenomenon may be of wider significance within the theory of vibration of thin, shallow shells, and the particular case which we treat here, both theoretically and experimentally, appears to be the simplest problem of this class.

The system that we consider is an elastic strip of uniform width and thickness (small compared with the width), bent along generators running across the width into a shape with a radius of curvature varying in some specified way along the length. We imagine the strip permanently bent to this shape, executing small vibrations about the position described. The two long edges are free, while the boundary conditions on the two ends will presumably not matter much when mode confinement occurs. In the original musical saw problem, the saw is vibrating about a position with non-zero mean stresses, since it is not permanently bent into the S-shape, but is held like that against elastic restoring forces. However, the model for the confinement behaviour which we advance depends only on the shape in the equilibrium position, so we treat as a canonical problem the permanently bent strip with no mean stress.

We first consider the vibration–transmission properties of such a strip with constant curvature (i.e. a section of cylindrical shell), then develop the theory of slowly varying curvature. From this we can deduce the conditions under which the confinement phenomenon occurs, and the frequencies and mode shapes of confined modes. An experimental investigation of the same problem is then described, and the predictions are tested against the experimental results. The level of agreement is found to be good.

The geometry, coordinate system and some essential notation are shown in figure 1. A strip of width $2a$ and thickness h has a curvature κ, which will in general vary slowly along the strip. The Young's modulus is denoted by E, Poisson's ratio σ, and density ρ. At a given point on the strip we use local cartesian coordinates x (along the strip), y (across the width) and z (normal to the surface). Corresponding components of shell displacement are denoted u_x, u_y and w respectively. The use of such local cartesian coordinates is one of the normal ingredients of shallow shell theory. Note that our particular geometry, with a developable surface, allows this without any distortion to the cartesian grid when it is deformed to follow the surface. We will assume throughout a harmonic time dependence of all displacement components, proportional to $e^{-i\omega t}$.

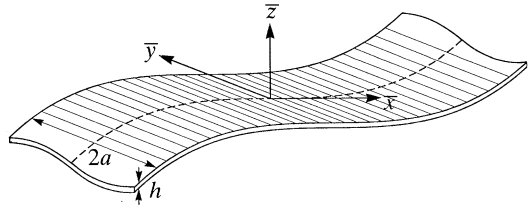

Figure 1. Sketch of the strip geometry, showing the coordinate system used.

The analysis to be described is based on Hamilton's principle. (The same results may also be derived using the equations of motion and boundary conditions for the system, but at greater length.) We begin from the lagrangian density L specified in terms of the quantities just defined. Our main interest lies in the motion normal to the surface of the strip, w. In a flat plate, the normal motion and the in-surface motion decouple to give two separate mathematical problems. On a curved shell this separation does not occur, but for shallow shells the possible free motions can still be divided into two classes, one in which the dynamics are dominated by normal motion and the other dominated by in-surface motion. We are interested in the former class. In all modes of interest the values of u_x and u_y will be small compared with that of w, and we need only allow for them in the extensional strain energy, where they appear multiplied by a large coefficient (proportional to h rather than h^3). Their contributions to the bending strain energy and the kinetic energy will be neglected. These are the only assumptions we make, over and above the usual ones associated with smallness of the motion and thinness of the strip.

Throughout most of the analysis we will use non-dimensional quantities. These are denoted by an overbar and defined as follows. The coordinates, frequency and curvature become

$$\bar{x} = x/a, \quad \bar{y} = y/a, \tag{1.1}$$

$$\bar{\omega} = (12(1-\sigma^2)\rho a^4/Eh^2)^{\frac{1}{2}}\omega \tag{1.2}$$

and

$$\bar{\kappa} = 12^{\frac{1}{2}}a^2\kappa/h \tag{1.3}$$

so that the strip occupies the domain $-1 \leqslant \bar{y} \leqslant 1$. There is no need to non-dimensionalize the vibrational displacements, but the relative magnitudes of in-plane and out-of-plane values are scaled according to

$$\bar{w} = w \tag{1.4}$$

and

$$\bar{u}_x = 12^{\frac{1}{2}}au_x/h, \tag{1.5}$$

$$\bar{u}_y = 12^{\frac{1}{2}}au_y/h. \tag{1.6}$$

The above frequency scaling was chosen so that the flat-strip waveguide cut-on frequencies occur at fixed numerical values of $\bar{\omega}$. The curvature scaling factor was chosen so that values of $\bar{\kappa}$ of order unity lead to significant, but not dominant, effects of curvature.

With the above non-dimensional quantities, and with the assumptions already described, the lagrangian density for the strip is

$$\bar{L} = \sigma\bar{e}^*_{ii}\,\bar{e}_{jj} + (1-\sigma)\,\bar{e}^*_{ij}\,\bar{e}_{ij} + \sigma\bar{\gamma}^*_{ii}\,\bar{\gamma}_{jj} + (1-\sigma)\,\bar{\gamma}^*_{ij}\,\bar{\gamma}_{ij} - \bar{\omega}^2|\bar{w}|^2, \tag{1.7}$$

where

$$\bar{e}_{ij} = \frac{1}{2}\left(\frac{\partial\bar{u}_i}{\partial\bar{x}_j} + \frac{\partial\bar{u}_j}{\partial\bar{x}_i}\right) - \bar{\kappa}_{ij}\,\bar{w}, \tag{1.8}$$

$$\bar{\gamma}_{ij} = \partial^2\bar{w}/\partial\bar{x}_i\,\partial\bar{x}_j \tag{1.9}$$

and $\bar{\kappa}_{xx} = \bar{\kappa}$ with all other components of $\bar{\kappa}_{ij}$ zero. In the above equation the asterisk denotes a complex conjugate and a summation convention applies to the indices, running over the two in-surface coordinates.

A constant factor has been removed from each term in (1.7). This does not affect the equations resulting from the application of Hamilton's principle

$$\delta \int_{\bar{x}_1}^{\bar{x}_2} \int_{-1}^{1} \bar{L} \, \mathrm{d}\bar{y} \, \mathrm{d}\bar{x} = 0, \tag{1.10}$$

in which application the usual manipulations of the calculus of variations, involving integration by parts with respect to $\bar{y}$ and $\bar{x}$, may be invoked to remove derivatives from the variations. The result provides the equations of motion of the strip and the boundary conditions on the free edges $\bar{y} = \pm 1$. It should be noted that, since the edges at $\bar{x} = \bar{x}_1, \bar{x}_2$ are not free, the terms which integration by parts generates at these edges are simply ignored. This is a point that should be borne in mind throughout the analysis: we shall not draw attention to such manipulation in detail.

2. Wave propagation behaviour for constant curvature

The first step is to consider the problem of wave propagation along the strip, for the simplest case when the curvature is constant. In this case, a propagation mode on the strip may conveniently be written in the form

$$\begin{pmatrix} \bar{u}_x \\ \bar{u}_y \\ \bar{w} \end{pmatrix} = \mathrm{e}^{\mathrm{i}\bar{k}\bar{x}} \begin{pmatrix} -\mathrm{i}\bar{\psi}_x(\bar{y}) \\ \bar{\psi}_y(\bar{y}) \\ \bar{\psi}(\bar{y}) \end{pmatrix}, \tag{2.1}$$

where $\bar{\psi}_x$, $\bar{\psi}_y$ and $\bar{\psi}$ are three as yet undetermined functions of $\bar{y}$. This, when substituted into (1.7)–(1.9), leads to the lagrangian density

$$\begin{aligned} \bar{L} = {} & \sigma \left| \bar{k}\bar{\psi}_x - \bar{\kappa}\bar{\psi} + \frac{\mathrm{d}\bar{\psi}_y}{\mathrm{d}\bar{y}} \right|^2 + (1-\sigma)\left[|\bar{k}\bar{\psi}_x - \bar{\kappa}\bar{\psi}|^2 + \left| \frac{\mathrm{d}\bar{\psi}_y}{\mathrm{d}\bar{y}} \right|^2 + \frac{1}{2} \left| \bar{k}\bar{\psi}_y - \frac{\mathrm{d}\bar{\psi}_x}{\mathrm{d}\bar{y}} \right|^2 \right] \\ & + \sigma \left| \frac{\mathrm{d}^2\bar{\psi}}{\mathrm{d}\bar{y}^2} - \bar{k}^2\bar{\psi} \right|^2 + (1-\sigma)\left[\left| \frac{\mathrm{d}^2\bar{\psi}}{\mathrm{d}\bar{y}^2} \right|^2 + 2\bar{k}^2 \left| \frac{\mathrm{d}\bar{\psi}}{\mathrm{d}\bar{y}} \right|^2 + \bar{k}^4 |\bar{\psi}|^2 \right] - \bar{\omega}^2 |\bar{\psi}|^2, \end{aligned} \tag{2.2}$$

which may, in principle, be used to obtain the equations of motion of the strip and boundary conditions at $\bar{y} = \pm 1$ via the variational principle

$$\delta \int_{-1}^{1} \bar{L} \, \mathrm{d}\bar{y} = 0. \tag{2.3}$$

For given values of $\bar{k}$ and $\bar{\kappa}$, the above equations and boundary conditions form an eigenvalue problem for $\bar{\omega}$, which can take on a series of values corresponding to the different propagation modes of the strip. The eigenfrequencies $\bar{\omega}$ are real and the solutions $\bar{\psi}_x$, $\bar{\psi}_y$ and $\bar{\psi}$ are also real functions of $\bar{y}$ (once a possible complex constant has been extracted, as we shall henceforth assume). We choose to normalize the solutions such that

$$\int_{-1}^{1} \bar{\psi}^2 \, \mathrm{d}\bar{y} = 1. \tag{2.4}$$

We need to be able to compute these propagation modes and their associated dispersion relations. This is readily done directly from the lagrangian density (2.2) using the variational principle and a suitable set of trial functions. (Here, we use the variational principle in its familiar guise as Rayleigh's principle, to obtain approximate frequencies. This contrasts with the use of variational methods in the analytical development, where they are strictly equivalent to the use of equations of motion and boundary conditions, and are formally exact.) The free boundary conditions at $\bar{y} = \pm 1$ do not need to be explicitly incorporated: they are associated with the unconstrained stationary points of the lagrangian density, and so will arise automatically from the variational calculation. An approach which is very easy to program and which gives sufficiently accurate results for our present purpose is to use truncated power series in $\bar{y}$ for the three components of displacement. From the symmetry of the problem, the propagation modes divide into a class which is symmetric about $\bar{y} = 0$ and a class which is antisymmetric about there. These can be computed separately, by using either only even powers in $\bar{y}$ or only odd powers in $\bar{y}$ in a suitable combination. It will turn out that we are primarily interested in the symmetric modes, so we illustrate the procedure for that case.

An appropriate combination of series may be defined as follows:

$$\bar{\psi}_x = \sum_{n=0}^{N-1} a_n \bar{y}^{2n}, \quad \bar{\psi}_y = \sum_{n=1}^{N} a_{n+N} \bar{y}^{2n-1}, \quad \bar{\psi} = \sum_{n=0}^{N-1} b_n \bar{y}^{2n}, \tag{2.5}$$

where N is some truncation value to be determined by numerical experiments on convergence of the approximation. Substituting these into (2.2) and performing the integrals with respect to $\bar{y}$ term by term we obtain an expression for the lagrangian as a quadratic form in the coefficient vectors $\boldsymbol{a}$, $\boldsymbol{b}$ which we may write

$$\int_{-1}^{1} \bar{L}\, \mathrm{d}\bar{y} = [\boldsymbol{a}^t\, \boldsymbol{b}^t] \begin{bmatrix} A & B \\ B^t & C \end{bmatrix} \begin{bmatrix} \boldsymbol{a} \\ \boldsymbol{b} \end{bmatrix} - \bar{\omega}^2 [\boldsymbol{a}^t\, \boldsymbol{b}^t] \begin{bmatrix} 0 & 0 \\ 0 & T \end{bmatrix} \begin{bmatrix} \boldsymbol{a} \\ \boldsymbol{b} \end{bmatrix} \tag{2.6}$$

in terms of matrices of coefficients A, B, C and T. It follows from the variational principle that the best estimates of the coefficients satisfy

$$\begin{bmatrix} A & B \\ B^t & C \end{bmatrix} \begin{bmatrix} \boldsymbol{a} \\ \boldsymbol{b} \end{bmatrix} = \bar{\omega}^2 \begin{bmatrix} 0 & 0 \\ 0 & T \end{bmatrix} \begin{bmatrix} \boldsymbol{a} \\ \boldsymbol{b} \end{bmatrix}. \tag{2.7}$$

The vector $\boldsymbol{a}$ does not enter the kinetic energy term in the lagrangian. This is a consequence of our assumption that the in-surface components of displacement do not influence the dynamics of the motion: they simply take the values which minimize the elastic potential energy at any given instant in a form of static equilibrium. We take account of this by manipulating (2.7) to eliminate $\boldsymbol{a}$. From the top row of (2.7)

$$\boldsymbol{a} = -A^{-1} B \boldsymbol{b}, \tag{2.8}$$

so that from the second row

$$B^t \boldsymbol{a} + C \boldsymbol{b} = \bar{\omega}^2 T \boldsymbol{b},$$

it follows that

$$V \boldsymbol{b} = \bar{\omega}^2 T \boldsymbol{b}, \tag{2.9}$$

where

$$V = C - B^t A^{-1} B. \tag{2.10}$$

For given values of σ, $\bar{k}$ and $\bar{\kappa}$ it is a straightforward matter to determine the elements of the matrices T and V. A suitable routine for the generalized eigenvector

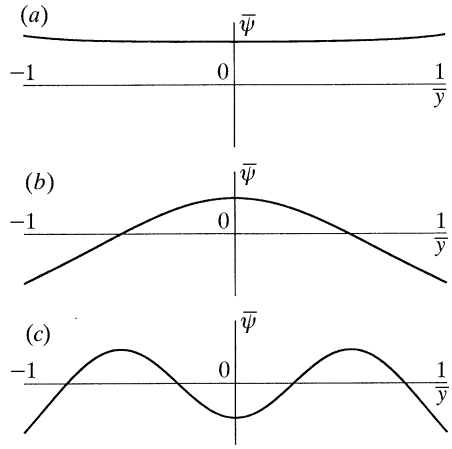

Figure 2. The normal component of displacement as a function of the dimensionless coordinate across the strip, for the first three symmetric waveguide modes of an elastic strip of constant curvature. Parameter values correspond to the experimental strip of §4, with a radius of curvature of 1 m and a dimensionless wavenumber $\bar{k} = \pi$.

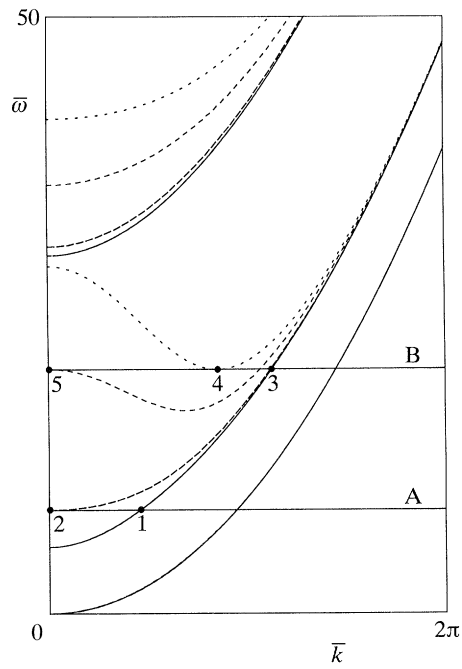

Figure 3. Dispersion curves for wave propagation along a strip of constant curvature, for the first three symmetric waveguide modes. Values of the dimensionless curvature parameter $\bar{\kappa}$ are as follows: solid lines $\bar{\kappa} = 0$; long dashes $\bar{\kappa} = 7$; medium dashes $\bar{\kappa} = 20.7$; short dashes $\bar{\kappa} = 30$.

problem may then be used to determine the set of mode shapes (via the coefficient vectors) and the frequency $\bar{\omega}$ of each. The antisymmetric modes may be similarly computed by replacing (2.5) with series approximations in which odd powers and even powers are interchanged.

Some results of such computations are shown in figures 2 and 3. These were calculated using the value $N = 7$, for which the approximations were found to have

converged adequately. Figure 2 shows the normal displacement function $\bar{\psi}$ for the first three symmetric modes of propagation, for some typical parameter values. As one might have anticipated, these functions look very reminiscent of free–free bending beam eigenmodes. Numerical experiments reveal that these shapes change only very slightly with wavenumber $\bar{k}$ and curvature $\bar{\kappa}$ within the range in which we will be interested. Figure 3 shows a set of dispersion characteristics for these symmetric modes. Wavenumber is plotted horizontally and frequency vertically. Curves are shown for the same three modes as plotted in figure 2, where these lie within the range of the graph. These curves have been calculated for several values of the non-dimensional curvature $\bar{\kappa}$, and these are all superimposed. Different line types are used for each value of $\bar{\kappa}$.

Solid lines correspond to zero curvature, in other words to a flat strip, and the behaviour revealed is just as one would guess. The lowest mode describes bending-beam motion of the whole strip, as can be seen from the displacement function in figure 2*a*, which is approximately uniform across the width. The corresponding dispersion curve shows the characteristic parabolic shape associated with bending beams or plates. It starts from the origin: there is no cut-on frequency for this mode. The higher waveguide modes have cut-on frequencies, corresponding to cross-sectional resonance with the appropriate shape, with no variation along the length of the strip. From these cut-on frequencies the curves rise monotonically, eventually asymptoting to the bending beam curve as axial bending comes to dominate the potential energy of the motion when the wavelength becomes short compared with the width of the strip, so that the precise cross-sectional shape ceases to matter very much.

The curves plotted in progressively shorter dashes correspond to increasing curvature of the strip, as specified in the caption. Towards the right-hand side of the picture, curvature is seen to have very little effect. On the left-hand side, however, there are very dramatic effects of curvature on the second mode, and rather less dramatic effects on the third mode. The bending-beam mode is hardly altered at all; so little, in fact, that at the resolution of figure 3 it is not possible to see that four curves are all plotted on top of one another. The second symmetric mode, which will turn out to be responsible for the audible confined mode of the saw, has its cut-on frequency raised very significantly by curvature, and with the higher values of curvature it assumes a shape which is no longer monotonic with wavenumber. The falling portion of the curve then indicates a situation in which the group velocity has the opposite sign to the phase velocity.

The peculiar shape of the dispersion curve for the second mode with high curvature can be explained qualitatively quite easily. For the flat plate, the vibration is inextensional at all frequencies and wavelengths. Introducing curvature necessitates some extensional motion in almost all cases, and thus raises frequencies to a greater or lesser extent depending on the amount of such motion needed. For the bending-beam mode, very little is needed. If the displacement were exactly uniform across the width of the strip, the motion would be exactly inextensional. This cannot quite be so because of edge effects associated with Poisson's ratio, but the raising of frequency is minimal. For the higher modes, though, there must be substantial amounts of extensional motion when the wavelength is long, and a dramatic rise in frequency is the result. As the wavelength decreases, the motion can adjust so that less longitudinal extension is needed, although at the expense of some in-surface shearing motion. This is the reason for the falling portion of the dispersion curve.

PHILOSOPHICAL TRANSACTIONS OF THE ROYAL SOCIETY A MATHEMATICAL, PHYSICAL & ENGINEERING SCIENCES

With even shorter wavelengths, the rising trend associated with bending takes over, and extensional effects cease to matter much.

Study of figure 3 allows us to give a qualitative explanation for the mode confinement phenomenon, if we argue that the curves plotted there will still have approximate local validity when the curvature is varying slowly with position. In §3, detailed analysis of the problem will support and extend this simple description. It was stated earlier that the confinement effect appears when the saw is bent into an S-shape. Such a shape has zero curvature at the inflection point, and curvature monotonically increasing in magnitude away from that point in both directions. For the simple model of the saw as a uniform beam in static equilibrium under end moments, the curvature would vary linearly with axial distance.

Assuming such a variation of curvature along our strip, suppose that we drive it at a frequency corresponding to the horizontal line labelled A in figure 3, in such a way as to excite the second symmetric mode of propagation only. At the inflection point, where the curvature is zero, this mode can propagate with a wavenumber corresponding to the point labelled 1. As it travels away from the centre, it encounters steadily increasing curvature. The frequency is fixed, so the wavenumber must vary so that at each point the dispersion relation appropriate to the local curvature is satisfied. From the behaviour of the family of dispersion curves we see that this cannot continue indefinitely. The wave will reach a point with a curvature corresponding to the first dashed curve in figure 3, labelled 2, and by then the wavenumber has become zero. Beyond that point, the curvature is too high for a wave of this type to propagate at all, so the wave must be reflected in some way near this critical point, and travel back towards the inflection point. It then passes through, and meets increasing curvature again on the other side. It will reflect again from the corresponding critical point, and repeat the process. It is immediately plausible that trapped modes can arise by this mechanism, at frequencies such that the total phase increase on a round trip is an integer multiple of 2π.

A rather more complicated sequence of events occurs at higher frequencies such as that corresponding to the horizontal line labelled B in figure 3. In this region of the diagram the dispersion curves display a falling then rising shape, which has implications for the form of confined modes. The wave this time leaves the point of inflection with the wavenumber given by the point labelled 3. It then travels unimpeded until it reaches the rather high curvature corresponding to the point labelled 4, at a minimum of the curve. Here it must reflect, as before. Since the group velocity must change sign at this reflection, the reflected wave follows the branch of the dispersion curve to the left of the minimum point 4. It can then travel back towards the inflection point, traversing the falling portion of the dispersion curve, but before it reaches the inflection it encounters another critical point, labelled 5, where the fixed frequency corresponds to the cut-on for this waveguide branch. Here it must reflect outwards again. It returns to the first critical point and reflects inwards again, now on the rising portion of the dispersion curve to the right of the point 4. It can then propagate all the way back to the centre, and out on the other side to repeat the whole complicated process there. Trapped modes can still arise, but with a more complicated spatial variation than that of the lower-frequency modes described above.

The vibration mode usually used when playing the musical saw turns out to be the first trapped mode for the second symmetric waveguide branch. This is illustrated in the holographic interferogram shown in figure 4. It is far from obvious that the

PHILOSOPHICAL TRANSACTIONS OF THE ROYAL SOCIETY A MATHEMATICAL, PHYSICAL & ENGINEERING SCIENCES

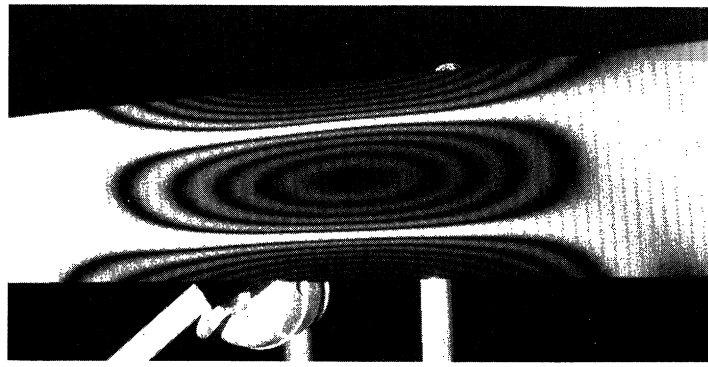

Figure 4. Holographic interferogram of the first confined mode on an S-shaped elastic strip, corresponding to the second symmetric waveguide branch. The strip is a different one from that studied experimentally in this paper, but the behaviour is very similar. Photograph kindly provided by Dr B. E. Richardson.

'slowly varying travelling wave' description just used to give a qualitative account of mode trapping is applicable to this mode, but the theory to be developed in §3 will extend to this case and allow the frequency and mode shape of such modes to be calculated.

3. Asymptotic analysis of trapped modes with slowly varying curvature

We now proceed to a more formal analysis of trapped modes on the strip. The analysis is based on the precept that the curvature $\bar{\kappa}$ is slowly varying with respect to $\bar{x}$. Formally we assume that

$$\bar{\kappa} = \bar{\kappa}(X), \tag{3.1}$$

where $X = \epsilon\bar{x}$ is a 'slow variable', that is one which varies slowly with $\bar{x}$, and ϵ is a small quantity upon which we form asymptotics as $\epsilon \to 0$. Our main concern is for the case when $\bar{\kappa}$ varies linearly with X, but we shall maintain as general a functional form for $\bar{\kappa}(X)$ as is consistent with simplicity of presentation. We will none the less assume that $\mathrm{d}\bar{\kappa}/\mathrm{d}X \neq 0$ and without loss of generality that $\mathrm{d}\bar{\kappa}/\mathrm{d}X > 0$.

As was explained in §2, our aim is to describe those modes of vibration which are trapped near a point of zero curvature. There could be a series of such trapped modes associated with each of the branches of the dispersion relation of a strip of constant curvature (with the exception of the lowest-frequency symmetric mode, discussed in §5, and the in-plane modes which are, in any case, not described by shallow shell theory). The modal series for a particular branch begins just above the flat strip cut-on frequency for the branch and the first few modes in the series are confined near the point of zero curvature. Higher modes become less closely confined and are described by slowly modulated waves reflected from points of zero group velocity.

This section provides quantitative analysis of each of the above types of behaviour. First, the modes near to the cut-on frequency are investigated. The higher modes require the solution of the problems of wave propagation between the points of reflection and analysis of the reflection problem itself. In each case, the method used consists of a perturbation expansion in powers of ϵ for the lagrangian. These expansions are derived from appropriate scalings for the coordinate $\bar{x}$ and asymptotic expansions of each of the vibrational quantities, u_x, u_y and w.

PHILOSOPHICAL TRANSACTIONS OF THE ROYAL SOCIETY A MATHEMATICAL, PHYSICAL & ENGINEERING SCIENCES

(a) *Further results for constant curvature*

Before embarking on the asymptotic analysis, we develop some results which we shall need by extending the constant-curvature analysis of §2. The dispersion properties of the propagation modes on the constant-curvature strip can be described by

$$\bar{\omega}^2 = \bar{D}(\bar{k}, \bar{\kappa}), \tag{3.2}$$

where it will prove useful to express $\bar{D}$ via (2.2) and $\int_{-1}^{1} \bar{L}\,\mathrm{d}\bar{y} = 0$ (which applies when the true eigenmodes are used) as

$$\bar{D} = \int_{-1}^{1} \sigma\left(\bar{k}\bar{\psi}_x - \bar{\kappa}\bar{\psi} + \frac{\mathrm{d}\bar{\psi}_y}{\mathrm{d}\bar{y}}\right)^2 + (1-\sigma)\left[(\bar{k}\bar{\psi}_x - \bar{\kappa}\bar{\psi})^2 + \left(\frac{\mathrm{d}\bar{\psi}_y}{\mathrm{d}\bar{y}}\right)^2 + \frac{1}{2}\left(\bar{k}\bar{\psi}_y - \frac{\mathrm{d}\bar{\psi}_x}{\mathrm{d}\bar{y}}\right)^2\right]$$
$$+ \sigma\left(\frac{\mathrm{d}^2\bar{\psi}}{\mathrm{d}\bar{y}^2} - \bar{k}^2\bar{\psi}\right)^2 + (1-\sigma)\left[\left(\frac{\mathrm{d}^2\bar{\psi}}{\mathrm{d}\bar{y}^2}\right)^2 + 2\bar{k}^2\left(\frac{\mathrm{d}\bar{\psi}}{\mathrm{d}\bar{y}}\right)^2 + \bar{k}^4\bar{\psi}^2\right]\mathrm{d}\bar{y}. \tag{3.3}$$

We may attribute a group velocity, $\bar{c}_{\mathrm{g}}$, to the modes using (3.2):

$$2\bar{\omega}\bar{c}_{\mathrm{g}} = \partial\bar{D}/\partial\bar{k} \tag{3.4}$$

and as always, the group velocity gives the speed of energy transport. Since the right-hand side of (3.3) is stationary with respect to variations of $\bar{\psi}_x$, $\bar{\psi}_y$ and $\bar{\psi}$ subject to (2.4), we may differentiate (3.3) with respect to $\bar{k}$ to obtain

$$\bar{\omega}\bar{c}_{\mathrm{g}} = \int_{-1}^{1} \bar{\psi}_x\left[\bar{k}\bar{\psi}_x - \bar{\kappa}\bar{\psi} + \sigma\frac{\mathrm{d}\bar{\psi}_y}{\mathrm{d}\bar{y}}\right] + \tfrac{1}{2}(1-\sigma)\,\bar{\psi}_y\left[\bar{k}\bar{\psi}_y - \frac{\mathrm{d}\bar{\psi}_x}{\mathrm{d}\bar{y}}\right]$$
$$- 2\bar{k}\bar{\psi}\left[\sigma\frac{\mathrm{d}^2\bar{\psi}}{\mathrm{d}\bar{y}^2} - \bar{k}^2\bar{\psi}\right] + 2(1-\sigma)\,\bar{k}\left(\frac{\mathrm{d}\bar{\psi}}{\mathrm{d}\bar{y}}\right)^2\mathrm{d}\bar{y}, \tag{3.5}$$

an expression we will need later in our analysis of wave propagation with slowly varying $\bar{\kappa}$.

We may also differentiate (3.3) with respect to $\bar{\kappa}$ to obtain

$$\frac{\partial\bar{D}}{\partial\bar{\kappa}} = -2\int_{-1}^{1} \bar{\psi}\left[\bar{k}\bar{\psi}_x - \bar{\kappa}\bar{\psi} + \sigma\frac{\mathrm{d}\bar{\psi}_y}{\mathrm{d}\bar{y}}\right]\mathrm{d}\bar{y}, \tag{3.6}$$

from which we wish first to show that $\bar{\kappa}\,\partial\bar{D}/\partial\bar{\kappa} \geqslant 0$ (again for future reference). To do this we exploit the fact that $\delta\int_{-1}^{1} \bar{L}\,\mathrm{d}\bar{y} = 0$ for any variation $\delta\bar{\psi}$. In particular if we set $\delta\bar{\psi} = \bar{\psi}$ we can show that (3.6) becomes

$$\tfrac{1}{2}\bar{\kappa}\frac{\partial\bar{D}}{\partial\bar{\kappa}} = \int_{-1}^{1} \sigma\left[\bar{k}\bar{\psi}_x - \bar{\kappa}\bar{\psi} + \frac{\mathrm{d}\bar{\psi}_y}{\mathrm{d}\bar{y}}\right]^2\mathrm{d}\bar{y}$$
$$+ (1-\sigma)\int_{-1}^{1}\left[(\bar{k}\bar{\psi}_x - \bar{\kappa}\bar{\psi})^2 + \left(\frac{\mathrm{d}\bar{\psi}_y}{\mathrm{d}\bar{y}}\right)^2 + \frac{1}{2}\left(\bar{k}\bar{\psi}_y - \frac{\mathrm{d}\bar{\psi}_x}{\mathrm{d}\bar{y}}\right)^2\right]\mathrm{d}\bar{y}, \tag{3.7}$$

which, being positive, demonstrates that the frequency of a given mode of propagation, at constant $\bar{k}$, increases with increasing $|\bar{\kappa}|$. This was illustrated by the dispersion curves shown in §2.

PHILOSOPHICAL TRANSACTIONS OF THE ROYAL SOCIETY A MATHEMATICAL, PHYSICAL & ENGINEERING SCIENCES

We now ask under what circumstances it is possible to have $\partial\bar{D}/\partial\bar{\kappa} = 0$ rather than being strictly positive. From (3.7) this happens when

$$\mathrm{d}\bar{\psi}_y/\mathrm{d}\bar{y} = 0, \tag{3.8}$$

$$\mathrm{d}\bar{\psi}_x/\mathrm{d}\bar{y} = \bar{k}\bar{\psi}_y \tag{3.9}$$

and

$$\bar{\kappa}\bar{\psi} = \bar{k}\bar{\psi}_x, \tag{3.10}$$

i.e. the in-plane strains are zero. Equation (3.8) shows that $\bar{\psi}_y$ is constant, while (3.9) leads to $\bar{\psi}_x = \bar{k}\bar{\psi}_y\,\bar{y} + C$. If $\bar{\kappa} \neq 0$, (3.10) can then be written as

$$\bar{\psi} = (\bar{k}/\bar{\kappa})\,(\bar{k}\bar{\psi}_y\,\bar{y} + C). \tag{3.11}$$

Now the boundary conditions on $\bar{\psi}$ obtained from the variational principle applied to (2.2) are

$$\mathrm{d}^2\bar{\psi}/\mathrm{d}\bar{y}^2 = \sigma\bar{k}^2\bar{\psi} \tag{3.12}$$

and

$$\mathrm{d}^3\bar{\psi}/\mathrm{d}\bar{y}^3 = (2-\sigma)\,\bar{k}^2\,\mathrm{d}\bar{\psi}/\mathrm{d}\bar{y} \tag{3.13}$$

on $\bar{y} = \pm 1$. Equations (3.11), (3.12) and (3.13) are inconsistent unless $\bar{k} = 0$. We conclude that $\partial\bar{D}/\partial\bar{\kappa} = 0$ is only possible if either $\bar{k}$ or $\bar{\kappa}$ is zero.

The case of zero $\bar{k}$ is of interest, since it yields the cut-on frequencies. Examination of (2.2) shows that $\bar{\psi}_x$ is then decoupled from $\bar{\psi}$ and $\bar{\psi}_y$. Variation of $\bar{\psi}_y$ leads to

$$\mathrm{d}\bar{\psi}_y/\mathrm{d}\bar{y} = \sigma\bar{\kappa}\bar{\psi} \tag{3.14}$$

which may then be substituted back into (2.2) to show that

$$\bar{L} = (\mathrm{d}^2\bar{\psi}/\mathrm{d}\bar{y}^2)^2 + ((1-\sigma^2)\,\bar{\kappa}^2 - \bar{\omega}^2)\,\bar{\psi}^2, \tag{3.15}$$

for which the variational principle yields

$$\mathrm{d}^4\bar{\psi}/\mathrm{d}\bar{y}^4 + ((1-\sigma^2)\,\bar{\kappa}^2 - \bar{\omega}^2)\,\bar{\psi} = 0, \tag{3.16}$$

with boundary conditions

$$\mathrm{d}^2\bar{\psi}/\mathrm{d}\bar{y}^2 = \mathrm{d}^3\bar{\psi}/\mathrm{d}\bar{y}^3 = 0 \tag{3.17}$$

on $\bar{y} = \pm 1$. This problem is essentially the classical free–free beam problem for which the frequencies are given in Rayleigh (1894). Thus

$$\bar{\omega}^2 = (1-\sigma^2)\,\bar{\kappa}^2 + \tfrac{1}{16}m^4 \tag{3.18}$$

with m given in article 174 of the above reference for the first five beam modes. Equation (3.18) provides the frequencies corresponding to strip propagation modes for $\bar{k} = 0$, i.e. the cut-on frequencies. The value $m = 0$ can also be introduced, to represent the lowest frequency anti-symmetric branch. The lowest symmetric branch is not covered by the above analysis and always lies at $\bar{\omega} = 0$ when $\bar{k} = 0$ (the limit as $\bar{k} \to 0$ is non-uniform for this branch).

From the above considerations we see that $\partial\bar{D}/\partial\bar{\kappa} = 0$ can only occur if $\bar{\kappa} = 0$, except for the lowest symmetric branch when either $\bar{k} = 0$ or $\bar{\kappa} = 0$ suffice. It remains to show that the converse is true, namely that $\partial\bar{D}/\partial\bar{\kappa} = 0$ when $\bar{\kappa} = 0$. In this case, the variational principle for $\bar{\psi}_x$ and $\bar{\psi}_y$ shows that $\bar{\psi}_x = \mathrm{d}\bar{\psi}_y/\mathrm{d}\bar{y} = 0$ and so (3.6) yields the required result.

This completes the analysis of the strip with constant curvature. We now proceed to the analysis of the strip with slowly varying curvature, for which a qualitative description has been given in §2.

(b) *The lower trapped modes*

Each trapped mode sequence begins somewhere near and above the frequency corresponding to $\bar{\kappa} = 0$, $\bar{k} = 0$; thus it follows from (3.18) that the mode sequence characterized by m starts a little above the frequency

$$\bar{\omega}_0 = \tfrac{1}{4}m^2. \tag{3.19}$$

The modes are trapped near the point X_0 at which $\bar{\kappa}(X_0) = 0$. We define $\hat{X} = (X - X_0)/\epsilon^{\frac{1}{2}}$ as a suitable scaling for the trapped modes. Note that we are not here concerned with the lowest symmetric branch of the dispersion relation, since this branch never forms trapped normal modes of the strip. The behaviour of modes based on this branch does nevertheless display some points of interest, which are discussed in §5.

The vibrational displacements are written in the form

$$\bar{u}_x = -\mathrm{i}U(\hat{X}, \bar{y}), \tag{3.20}$$

$$\bar{u}_y = V(\hat{X}, \bar{y}), \tag{3.21}$$

$$\bar{w} = W(\hat{X}, \bar{y}), \tag{3.22}$$

and each of U, V and W is expanded as an asymptotic series in $\epsilon^{\frac{1}{2}}$, for instance

$$U = U^{(0)} + \epsilon^{\frac{1}{2}}U^{(1)} + \epsilon U^{(2)} + o(\epsilon). \tag{3.23}$$

Furthermore, since we are looking for normal modes of as yet unknown frequency

$$\bar{\omega}^2 = \bar{\omega}_0^2 + \epsilon\Omega_1 + o(\epsilon). \tag{3.24}$$

The curvature, $\bar{\kappa}$, can also be expanded via

$$\bar{\kappa} = \epsilon^{\frac{1}{2}}\bar{\kappa}_0'\hat{X} + o(\epsilon^{\frac{1}{2}}), \tag{3.25}$$

where $\bar{\kappa}_0' = \mathrm{d}\bar{\kappa}(X_0)/\mathrm{d}X$.

The scaling for X and the expansions we have introduced may appear somewhat *ad hoc*. In fact they are based on the analysis to follow. Incorrect approaches lead to trivial or contradictory results, the scalings and expansions being, in practice, determined by trial and error. The same general principles apply in each of the cases we will study.

The above expansions for $\bar{u}_x$, $\bar{u}_y$, $\bar{w}$, $\bar{\kappa}$ and $\bar{\omega}^2$ are substituted into (1.7)–(1.9). The leading-order expression for the lagrangian density which results is

$$\bar{L}^{(0)} = \left|\frac{\partial V^{(0)}}{\partial \bar{y}}\right|^2 + \tfrac{1}{2}(1-\sigma)\left|\frac{\partial U^{(0)}}{\partial \bar{y}}\right|^2 + \left|\frac{\partial^2 W^{(0)}}{\partial \bar{y}^2}\right|^2 - \bar{\omega}_0^2|W^{(0)}|^2, \tag{3.26}$$

from which the variational principle leads to

$$\partial U^{(0)}/\partial \bar{y} = \partial V^{(0)}/\partial \bar{y} = 0 \tag{3.27}$$

and

$$\partial^4 W^{(0)}/\partial \bar{y}^4 - \bar{\omega}_0^2 W^{(0)} = 0, \tag{3.28}$$

with boundary conditions

$$\partial^2 W^{(0)}/\partial \bar{y}^2 = \partial^3 W^{(0)}/\partial \bar{y}^3 = 0 \tag{3.29}$$

on $\bar{y} = \pm 1$. These equations show that $W^{(0)}$ is the free–free beam function, as was to be expected given the analysis of the case $\bar{k} = 0$ before. Thus

$$W^{(0)} = A(\hat{X})\,\bar{\psi}^{(0)}(\bar{y}), \tag{3.30}$$

where $\bar{\psi}^{(0)}$ denotes the beam function normalized according to (2.4). The quantities $U^{(0)}$ and $V^{(0)}$ are functions of $\hat{X}$ alone. The solution at leading order has therefore been determined up to the unknown functions $A(\hat{X})$, $U^{(0)}(\hat{X})$ and $V^{(0)}(\hat{X})$, which we are still at liberty to use in variational arguments at higher order in the expansion of $\bar{L}$.

At the next order in the expansion

$$\bar{L} = \bar{L}^{(0)} + \epsilon^{\frac{1}{2}}\bar{L}^{(1)} + \epsilon\bar{L}^{(2)} + o(\epsilon) \tag{3.31}$$

of the lagrangian density we find that $\int_{-1}^{1} \bar{L}^{(1)}\,\mathrm{d}\bar{y}$ is identically zero by virtue of the leading order equations (3.27)–(3.29). The next term is

$$\begin{aligned}\int_{-1}^{1} \bar{L}^{(2)}\,\mathrm{d}\bar{y} = \int_{-1}^{1} \sigma \left|\frac{\partial V^{(1)}}{\partial \bar{y}} - \bar{\kappa}_0' \hat{X} W^{(0)} - \mathrm{i}\frac{\mathrm{d}U^{(0)}}{\mathrm{d}\hat{X}}\right|^2 \\ + (1-\sigma)\left[\left|\bar{\kappa}_0' \hat{X} W^{(0)} + \mathrm{i}\frac{\mathrm{d}U^{(0)}}{\mathrm{d}\hat{X}}\right|^2 + \left|\frac{\partial V^{(1)}}{\partial \bar{y}}\right|^2 + \frac{1}{2}\left|\frac{\partial U^{(1)}}{\partial \bar{y}} + \mathrm{i}\frac{\mathrm{d}V^{(0)}}{\mathrm{d}\hat{X}}\right|^2\right] \\ + \sigma\left[\frac{\partial^2 W^{(0)}}{\partial \hat{X}^2}\frac{\partial^2 W^{(0)*}}{\partial \bar{y}^2} + \frac{\partial^2 W^{(0)*}}{\partial \hat{X}^2}\frac{\partial^2 W^{(0)}}{\partial \bar{y}^2}\right] \\ + 2(1-\sigma)\left|\frac{\partial^2 W^{(0)}}{\partial \hat{X}\,\partial \bar{y}}\right|^2 + \left|\frac{\partial^2 W^{(1)}}{\partial \bar{y}^2}\right|^2 - \bar{\omega}_0^2 |W^{(1)}|^2 - \Omega_1 |W^{(0)}|^2\,\mathrm{d}\bar{y}. \end{aligned} \tag{3.32}$$

We use the variational principle

$$\delta \int_{\hat{x}_1}^{\hat{x}_2} \int_{-1}^{1} \bar{L}^{(2)}\,\mathrm{d}\bar{y}\,\mathrm{d}\hat{X} = 0 \tag{3.33}$$

and first consider variations of $U^{(1)}$, $V^{(1)}$ and $W^{(1)}$. These lead to

$$\partial U^{(1)}/\partial \bar{y} + \mathrm{i}\,\mathrm{d}V^{(0)}/\mathrm{d}\hat{X} = 0, \tag{3.34}$$

$$\partial V^{(1)}/\partial \bar{y} = \sigma(\bar{\kappa}_0' \hat{X} W^{(0)} + \mathrm{i}(\mathrm{d}U^{(0)}/\mathrm{d}\hat{X})) \tag{3.35}$$

and $W^{(1)}$ satisfies the free–free beam problem, (3.28) and (3.29), in place of $W^{(0)}$. When (3.34), (3.35) and the conditions on $W^{(1)}$ are used in (3.32) we find

$$\begin{aligned}\int_{-1}^{1} \bar{L}^{(2)}\,\mathrm{d}\bar{y} = \int_{-1}^{1} (1-\sigma^2)\left|\bar{\kappa}_0' \hat{X} W^{(0)} + \mathrm{i}\frac{\mathrm{d}U^{(0)}}{\mathrm{d}\hat{X}}\right|^2 + \sigma\left[\frac{\partial^2 W^{(0)}}{\partial \hat{X}^2}\frac{\partial^2 W^{(0)*}}{\partial \bar{y}^2} + \frac{\partial^2 W^{(0)*}}{\partial \hat{X}^2}\frac{\partial^2 W^{(0)}}{\partial \bar{y}^2}\right] \\ + 2(1-\sigma)\left|\frac{\partial^2 W^{(0)}}{\partial \hat{X}\,\partial \bar{y}}\right|^2 - \Omega_1 |W^{(0)}|^2\,\mathrm{d}\bar{y}. \end{aligned} \tag{3.36}$$

The variational principle (3.33), (3.36), allowing for variations of $U^{(0)}(\hat{X})$, leads to

$$2\mathrm{i}\frac{\mathrm{d}U^{(0)}}{\mathrm{d}\hat{X}} + \hat{X}\bar{\kappa}_0' \int_{-1}^{1} W^{(0)}\,\mathrm{d}\bar{y} = 0. \tag{3.37}$$

For non-zero $\bar{\omega}_0^2$ it follows from (3.28) and (3.29) that

$$\int_{-1}^{1} W^{(0)}\,\mathrm{d}\bar{y} = 0 \tag{3.38}$$

and this also holds when $\bar{\omega}_0^2 = 0$ since the mode in question is then the lowest *antisymmetric* branch. Equation (3.37) therefore yields

$$\mathrm{d}U^{(0)}/\mathrm{d}\hat{X} = 0, \tag{3.39}$$

which we can use, along with (3.30), to write (3.36) as

$$\int_{-1}^{1} \bar{L}^{(2)}\,\mathrm{d}\bar{y} = \sigma \int_{-1}^{1} \bar{\psi}^{(0)} \frac{\mathrm{d}^2\bar{\psi}^{(0)}}{\mathrm{d}\bar{y}^2}\,\mathrm{d}\bar{y}\left[\frac{\mathrm{d}^2 A}{\mathrm{d}\hat{X}^2}A^* + \frac{\mathrm{d}^2 A^*}{\mathrm{d}\hat{X}^2}A\right]$$
$$+ 2(1-\sigma)\int_{-1}^{1}\left(\frac{\mathrm{d}\bar{\psi}^{(0)}}{\mathrm{d}\bar{y}}\right)^2 \mathrm{d}\bar{y}\left|\frac{\mathrm{d}A}{\mathrm{d}\hat{X}}\right|^2 + (\bar{\kappa}_0'^2(1-\sigma^2)\hat{X}^2 - \Omega_1)|A|^2, \quad (3.40)$$

which only contains the one unknown quantity, $A(\hat{X})$.

The final step in the analysis is to consider the variational principle (3.33), (3.40) with $A(\hat{X})$ allowed to vary. Ignoring terms at $\hat{X} = \hat{X}_1, \hat{X}_2$ which are introduced by integration by parts, we find that

$$\alpha^2\,\mathrm{d}^2A/\mathrm{d}\hat{X}^2 - ((1-\sigma^2)\bar{\kappa}_0'^2\hat{X}^2 - \Omega_1)A = 0, \quad (3.41)$$

where $\alpha > 0$ is given by

$$\alpha^2 = 2\int_{-1}^{1}(1-\sigma)\left(\frac{\mathrm{d}\bar{\psi}^{(0)}}{\mathrm{d}\bar{y}}\right)^2 - \sigma\bar{\psi}^{(0)}\frac{\mathrm{d}^2\bar{\psi}^{(0)}}{\mathrm{d}\bar{y}^2}\,\mathrm{d}\bar{y}. \quad (3.42)$$

Equation (3.41) describes the modes trapped near the point $X = X_0$. It is the Schrödinger equation for a harmonic oscillator (see, for example, Pippard 1983), and has eigenvalues

$$\Omega_1 = (2n+1)(1-\sigma^2)^{\frac{1}{2}}\alpha\bar{\kappa}_0', \quad (3.43)$$

with corresponding eigensolutions

$$A = \mathrm{e}^{-\bar{\mu}^2\hat{X}^2/2}H_n(\bar{\mu}\hat{X}), \quad (3.44)$$

where H_n is a Hermite polynomial and

$$\bar{\mu} = ((1-\sigma^2)\bar{\kappa}_0'^2/\alpha^2)^{\frac{1}{4}}. \quad (3.45)$$

The integer n labels the modes in the series considered, $n = 0$ being the lowest frequency. We note that the frequency spacing of the modes is constant to the order we are working

$$\Delta\bar{\omega} = \epsilon(1-\sigma^2)^{\frac{1}{2}}\bar{\kappa}_0'\alpha/\bar{\omega}_0, \quad (3.46)$$

with the exception of the lowest antisymmetric branch, for which $\bar{\omega}$ is proportional to $(2n+1)^{\frac{1}{2}}$.

The quantity α is defined by (3.42) and for the lowest antisymmetric branch ($m = 0$) may be easily calculated as $\alpha^2 = 6(1-\sigma)$. For the higher branches we proceed as follows. Integration by parts of the second term of the integrand of (3.42) yields

$$\alpha^2 = 2\int_{-1}^{1}\left(\frac{\mathrm{d}\bar{\psi}^{(0)}}{\mathrm{d}\bar{y}}\right)^2\mathrm{d}\bar{y} - 2\sigma\left[\bar{\psi}_0\frac{\mathrm{d}\bar{\psi}_0}{\mathrm{d}\bar{y}}\right]_{-1}^{1} \quad (3.47)$$

and we note (see Rayleigh 1894, article 164) that

$$2\int_{-1}^{1}\left(\frac{\mathrm{d}\bar{\psi}^{(0)}}{\mathrm{d}\bar{y}}\right)^2\mathrm{d}\bar{y} = 3\bar{\psi}_0(1)\frac{\mathrm{d}\bar{\psi}^{(0)}}{\mathrm{d}\bar{y}}(1) + \left(\frac{\mathrm{d}\bar{\psi}^{(0)}}{\mathrm{d}\bar{y}}\right)^2(1) \quad (3.48)$$

and

$$\int_{-1}^{1}\bar{\psi}^{(0)\,2}\,\mathrm{d}\bar{y} = \tfrac{1}{2}\bar{\psi}^{(0)\,2}(1) = 1. \quad (3.49)$$

Table 1. *Values of m and α for the first six confined branches, calculated using $\sigma = 0.28$*

m	α
0	4.32
4.73	4.42
7.85	6.76
11.00	9.01
14.14	11.25
17.28	13.48

Let
$$\lambda = \frac{(\mathrm{d}\bar{\psi}^{(0)}(1)/\mathrm{d}\bar{y})}{\bar{\psi}^{(0)}(1)}, \tag{3.50}$$
then (3.47) becomes
$$\alpha^2 = 2\lambda(3-4\sigma+\lambda). \tag{3.51}$$

Now, the free–free beam problem (3.28) and (3.29) with $\bar{\omega}_0 = \frac{1}{4}m^2$ has the solution
$$\bar{\psi}_0 = A(\cos\tfrac{1}{2}m(\bar{y}-1)+\cosh\tfrac{1}{2}m(\bar{y}-1))+B(\sin\tfrac{1}{2}m(\bar{y}-1)+\sinh\tfrac{1}{2}m(\bar{y}-1)), \tag{3.52}$$
where we have arranged to satisfy the boundary conditions on $\bar{y} = 1$. The condition that $\mathrm{d}^2\bar{\psi}^{(0)}/\mathrm{d}\bar{y}^2 = 0$ on $\bar{y} = -1$ yields
$$A(\cosh m-\cos m) = B(\sinh m-\sin m), \tag{3.53}$$
which, together with (3.50) and (3.52) leads to
$$\lambda = \tfrac{1}{2}m\frac{\cosh m-\cos m}{\sinh m-\sin m}, \tag{3.54}$$
giving α in terms of m via (3.51). The first six values of m and α are listed in table 1 for a Poisson's ratio $\sigma = 0.28$ corresponding to a steel strip.

Although we do not present the analysis here, it can be extended to the next order in $\epsilon^{\frac{1}{2}}$. At order $\epsilon^{\frac{3}{2}}$ in $\bar{L}$, it turns out that the correction to $\bar{\omega}^2$, of order $\epsilon^{\frac{3}{2}}$, is zero.

This completes our analysis of the lower members of a series of trapped modes. When re-expressed in dimensional terms, the frequencies are given by
$$\omega^2 = \omega_0^2+(2n+1)\frac{Eh\alpha}{a\rho\sqrt{(12(1-\sigma^2))}}\frac{\mathrm{d}\kappa_0}{\mathrm{d}x}, \tag{3.55}$$
with
$$\omega_0 = \tfrac{1}{4}m^2(Eh^2/12(1-\sigma^2)\rho a^4)^{\frac{1}{2}}. \tag{3.56}$$
The frequency spacing is constant to the order of approximation to which we are working here, except in the case of the $m = 0$ series. Equation (3.46) can be expressed in dimensional form to give the mode spacing as
$$\Delta\omega = \frac{4\alpha}{m^2}\left(\frac{E}{\rho}\right)^{\frac{1}{2}}a\frac{\mathrm{d}\kappa_0}{\mathrm{d}x}, \tag{3.57}$$
with the first mode in the series at $\omega = \omega_0+\frac{1}{2}\Delta\omega$. The mode shapes are given by
$$A = \mathrm{e}^{-\mu^2(x-x_0)^2/2}H_n(\mu(x-x_0)) \tag{3.58}$$
where
$$\mu = (12(1-\sigma^2))^{\frac{1}{4}}\left(\frac{a}{h\alpha}\frac{\mathrm{d}\kappa_0}{\mathrm{d}x}\right)^{\frac{1}{2}}. \tag{3.59}$$

Before moving on to discuss the higher modes of the series, we should mention that mode trapping can also be shown to occur at any point of minimum $|\kappa|$. In general such points occur where $\mathrm{d}\kappa/\mathrm{d}x = 0$, a case we have specifically excluded. None the less it is worth stressing that modal traps are essentially positions where the curvature is a minimum. This can occur at positions of zero curvature as considered here, or at minima of non-zero curvature.

(c) *Wave propagation*

This subsection describes the analysis that is used to quantify the propagation of waves between reflection points. The essence of the method is the classical WKB approach which is based on slowly modulated waves whose wavenumber is determined locally as if the strip had constant curvature. The vibrational displacements are written as

$$\bar{u}_x = -\mathrm{i}U(X,\bar{y})\,\mathrm{e}^{\mathrm{i}\phi(X)/\epsilon}, \tag{3.60}$$

$$\bar{u}_y = V(X,\bar{y})\,\mathrm{e}^{\mathrm{i}\phi(X)/\epsilon}, \tag{3.61}$$

$$\bar{w} = W(X,\bar{y})\,\mathrm{e}^{\mathrm{i}\phi(X)/\epsilon}, \tag{3.62}$$

where $\phi(X)$ is a phase function which we choose to match the local wavenumber, i.e.

$$\mathrm{d}\phi/\mathrm{d}X = \bar{k}. \tag{3.63}$$

This description regards $\bar{k}$ as a function of X. We are not concerned with its functional dependence on $\bar{\omega}$, which is constant and regarded as given. Of course, the ultimate aim is to determine modal frequencies but this will only come about once we have developed the theory for the propagation and reflection of waves on the strip of slowly varying curvature.

Each of the quantities, U, V and W is expanded as an asymptotic series in ϵ, for instance

$$U = U^{(0)} + \epsilon U^{(1)} + o(\epsilon). \tag{3.64}$$

The leading order expression for the lagrangian is, as one might expect, given by (2.2). This means that the problem is locally determined by the theory for constant curvature and that

$$\begin{pmatrix} U^{(0)} \\ V^{(0)} \\ W^{(0)} \end{pmatrix} = A(X) \begin{pmatrix} \bar{\psi}_x(\bar{y}) \\ \bar{\psi}_y(\bar{y}) \\ \bar{\psi}(\bar{y}) \end{pmatrix}. \tag{3.65}$$

The next order term in the expansion of lagrangian density

$$\bar{L} = \bar{L}^{(0)} + \epsilon \bar{L}^{(1)} + o(\epsilon) \tag{3.66}$$

is

$$\begin{aligned} \int_{-1}^{1} \bar{L}^{(1)}\,\mathrm{d}\bar{y} = 2\int_{-1}^{1} \mathrm{Re}\Big\{ & \mathrm{i}\frac{\partial U^{(0)*}}{\partial X}\left[\bar{k}U^{(0)} - \bar{\kappa}W^{(0)} + \sigma\frac{\partial V^{(0)}}{\partial \bar{y}}\right] + \tfrac{1}{2}\mathrm{i}(1-\sigma)\frac{\partial V^{(0)*}}{\partial X} \\ & \times\left(\bar{k}V^{(0)} - \frac{\partial U^{(0)}}{\partial \bar{y}}\right) - \mathrm{i}\left(2\bar{k}\frac{\partial W^{(0)*}}{\partial X} + \frac{\partial \bar{k}}{\partial X}W^{(0)*}\right)\left(\sigma\frac{\partial^2 W^{(0)}}{\partial \bar{y}^2} - \bar{k}^2 W^{(0)}\right) \\ & + 2\mathrm{i}\bar{k}(1-\sigma)\frac{\partial W^{(0)}}{\partial \bar{y}}\frac{\partial^2 W^{(0)*}}{\partial X\,\partial \bar{y}}\Big\}\,\mathrm{d}\bar{y} \end{aligned} \tag{3.67}$$

and when (3.5) and (3.65) are used we obtain

$$\int_{-1}^{1} L^{(1)}\,\mathrm{d}\bar{y} = 2\bar{\omega}\bar{c}_{\mathrm{g}}\,\mathrm{Re}\left\{\mathrm{i}A\,\frac{\partial A^*}{\partial X}\right\} \tag{3.68}$$

from which the variational method leads to

$$\partial(A^2\bar{c}_{\mathrm{g}})/\partial X = 0. \tag{3.69}$$

This equation has two consequences. First, the magnitude $|A|^2\bar{c}_{\mathrm{g}}$ is constant. This result was, of course, to be expected from energy conservation arguments since the energy per unit length of strip is proportional to $|A|^2$. The second consequence is that the phase of the wave, perhaps somewhat surprisingly, undergoes no leading order change to the value determined by $\phi(X)/\epsilon$. Thus, in going from X_1 to X_2 the phase changes by

$$\frac{\phi(X_2)-\phi(X_1)}{\epsilon} = \int_{X_1}^{X_2} \bar{k}\,\mathrm{d}X + o(1). \tag{3.70}$$

(*d*) *Wave reflection*

The waves we have been describing are reflected at points for which $\bar{c}_{\mathrm{g}} = 0$. As in the classical WKB method it is necessary to describe these regions separately because the expansions we have adopted are no longer valid there: for instance (3.69) predicts an infinite value of the displacement amplitudes when $\bar{c}_{\mathrm{g}} = 0$. Suppose that $\bar{c}_{\mathrm{g}} = 0$ at $X = X_0$ so that wave reflection occurs there. Let $\bar{\kappa}_0$ and $\bar{k}_0$ be the corresponding values of $\bar{\kappa}$ and $\bar{k}$ (for the given value of $\bar{\omega}$). We further define $\bar{\psi}_x^{(0)}$, $\bar{\psi}_y^{(0)}$ and $\bar{\psi}^{(0)}$ to have the values they assume at $\bar{k} = \bar{k}_0$, $\bar{\kappa} = \bar{\kappa}_0$. Finally, the scaling for $\bar{x}$ is defined by

$$\tilde{X} = (X - X_0)/\epsilon^{\frac{2}{3}} \tag{3.71}$$

and the vibrational displacements are given by

$$\bar{u}_x = -\mathrm{i}\,\mathrm{e}^{\mathrm{i}\bar{k}_0\bar{x}}\,U(\tilde{X},\bar{y}), \tag{3.72}$$

$$\bar{u}_y = \mathrm{e}^{\mathrm{i}\bar{k}_0\bar{x}}\,V(\tilde{X},\bar{y}), \tag{3.73}$$

$$\bar{w} = \mathrm{e}^{\mathrm{i}\bar{k}_0\bar{x}}\,W(\tilde{X},\bar{y}), \tag{3.74}$$

where each of U, V and W is expanded in powers of $\epsilon^{\frac{1}{3}}$, for instance

$$U = U^{(0)} + \epsilon^{\frac{1}{3}}U^{(1)} + \epsilon^{\frac{2}{3}}U^{(2)} + o(\epsilon^{\frac{2}{3}}) \tag{3.75}$$

and the curvature has the form

$$\bar{\kappa} = \bar{\kappa}_0 + \epsilon^{\frac{2}{3}}\bar{\kappa}_0'\tilde{X} + o(\epsilon^{\frac{2}{3}}). \tag{3.76}$$

The leading order term in the expansion of lagrangian density is of no great surprise. It is given by (2.2) with $\bar{k}_0$ and $\bar{\kappa}_0$ in place of $\bar{k}$ and $\bar{\kappa}$. It follows that

$$\begin{pmatrix} U^{(0)} \\ V^{(0)} \\ W^{(0)} \end{pmatrix} = A(\tilde{X}) \begin{pmatrix} \bar{\psi}_x^{(0)}(\bar{y}) \\ \bar{\psi}_y^{(0)}(\bar{y}) \\ \bar{\psi}^{(0)}(\bar{y}) \end{pmatrix}. \tag{3.77}$$

The expansion of the lagrangian proceeds as

$$\bar{L} = \bar{L}^{(0)} + \epsilon^{\frac{1}{3}}\bar{L}^{(1)} + \epsilon^{\frac{2}{3}}\bar{L}^{(2)} + o(\epsilon^{\frac{2}{3}}) \tag{3.78}$$

and it turns out that $\int_{-1}^{1} \bar{L}^{(1)}\,\mathrm{d}\bar{y}$ is identically zero by virtue of the leading order variational problem being satisfied and because $\bar{c}_{\mathrm{g}} = 0$ at $X = X_0$ (cf. equation (3.5)).

The second-order term is given by

$$\bar{L}^{(2)} = \bar{L}_1^{(2)} + \bar{L}_2^{(2)}, \tag{3.79}$$

where $\bar{L}_1^{(2)}$ has the same form, (2.2), as $\bar{L}^{(0)}$ but with $U^{(1)}$, $V^{(1)}$ and $W^{(1)}$ in place of $\bar{\psi}_x$, $\bar{\psi}_y$ and $\bar{\psi}$ respectively (and of course with $\bar{k} = \bar{k}_0$, $\bar{\kappa} = \bar{\kappa}_0$). The other term is given by the somewhat lengthy expression

$$\begin{aligned}
\int_{-1}^{1} \bar{L}_2^{(2)}\,\mathrm{d}\bar{y} = 2\int_{-1}^{1} \mathrm{Re}\Bigg\{ & \left(\mathrm{i}\frac{\partial U^{(1)*}}{\partial \tilde{X}} - \bar{\kappa}_0' \tilde{X} W^{(0)*}\right)\left(\bar{k}_0 U^{(0)} - \bar{\kappa}_0 W^{(0)} + \sigma\frac{\partial V^{(0)}}{\partial \bar{y}}\right) \\
& - \mathrm{i}\frac{\partial U^{(0)}}{\partial \tilde{X}}\left(\bar{k}_0 U^{(1)*} - \bar{\kappa}_0 W^{(1)*} + \sigma\frac{\partial V^{(1)*}}{\partial \bar{y}}\right) \\
& + \tfrac{1}{2}\mathrm{i}(1-\sigma)\left[\frac{\partial V^{(1)*}}{\partial \tilde{X}}\left(\bar{k}_0 V^{(0)} - \frac{\partial U^{(0)}}{\partial \bar{y}}\right) - \frac{\partial V^{(0)}}{\partial \tilde{X}}\left(\bar{k}_0 V^{(1)*} - \frac{\partial U^{(1)*}}{\partial \bar{y}}\right)\right] \\
& + \left(\frac{\partial^2 W^{(0)*}}{\partial \tilde{X}^2} - 2\mathrm{i}\bar{k}_0\frac{\partial W^{(1)*}}{\partial \tilde{X}}\right)\left(\sigma\frac{\partial^2 W^{(0)}}{\partial \bar{y}^2} - \bar{k}_0^2 W^{(0)}\right) \\
& + 2\mathrm{i}\bar{k}_0\frac{\partial W^{(0)}}{\partial \tilde{X}}\left(\sigma\frac{\partial^2 W^{(1)*}}{\partial \bar{y}^2} - \bar{k}_0^2 W^{(1)*}\right) \\
& + 2\mathrm{i}\bar{k}_0(1-\sigma)\left(\frac{\partial W^{(0)}}{\partial \bar{y}}\frac{\partial^2 W^{(1)*}}{\partial \tilde{X}\,\partial \bar{y}} - \frac{\partial W^{(1)*}}{\partial \bar{y}}\frac{\partial^2 W^{(0)}}{\partial \tilde{X}\,\partial \bar{y}}\right)\Bigg\}\mathrm{d}\bar{y}.
\end{aligned} \tag{3.80}$$

When variations of $U^{(1)}$, $V^{(1)}$ and $W^{(1)}$ are carried out at this order, extremely lengthy equations result. We do not need to examine the details of these equations, but it is necessary to understand their general form. They consist of three linear differential equations for $U^{(1)}$, $V^{(1)}$ and $W^{(1)}$ as functions of $\bar{y}$ with four boundary conditions on each edge. Formally we may express the problem as

$$\Gamma\begin{pmatrix} U^{(1)} \\ V^{(1)} \\ W^{(1)} \end{pmatrix} = \mathrm{i}\frac{\partial A}{\partial \tilde{X}}\boldsymbol{\chi}, \tag{3.81}$$

where Γ is a real linear differential operator on $U^{(1)}(\bar{y})$, $V^{(1)}(\bar{y})$ and $W^{(1)}(\bar{y})$, while $\boldsymbol{\chi}$ is a vector of seven real-valued right-hand sides whose values are determined from the leading order quantities, $\bar{\psi}_x^{(0)}$, $\bar{\psi}_y^{(0)}$ and $\bar{\psi}^{(0)}$. The leading order equations are expressed by

$$\Gamma\begin{pmatrix} U^{(0)} \\ V^{(0)} \\ W^{(0)} \end{pmatrix} = 0. \tag{3.82}$$

The solution of (3.81) is indeterminate up to a multiple of the leading order solution $\bar{\psi}_x^{(0)}$, $\bar{\psi}_y^{(0)}$ and $\bar{\psi}^{(0)}$, and can be written in the form

$$\begin{pmatrix} U^{(1)} \\ V^{(1)} \\ W^{(1)} \end{pmatrix} = \mathrm{i}\frac{\partial A}{\partial \tilde{X}}\begin{pmatrix} \bar{\psi}_x^{(1)} \\ \bar{\psi}_y^{(1)} \\ \bar{\psi}^{(1)} \end{pmatrix} + A_1(\tilde{X})\begin{pmatrix} \bar{\psi}_x^{(0)} \\ \bar{\psi}_y^{(0)} \\ \bar{\psi}^{(0)} \end{pmatrix}, \tag{3.83}$$

where $\bar{\psi}_x^{(1)}$, $\bar{\psi}_y^{(1)}$ and $\bar{\psi}^{(1)}$ are any real-valued solution of

$$\Gamma\begin{pmatrix}\bar{\psi}_x^{(1)}\\ \bar{\psi}_y^{(1)}\\ \bar{\psi}^{(1)}\end{pmatrix} = \boldsymbol{\chi}. \tag{3.84}$$

When the formal solution (3.83) is substituted into $\bar{L}_1^{(2)}$ and $\bar{L}_2^{(2)}$ we find that the second term does not contribute and that

$$\int_{-1}^{1} \bar{L}^{(2)}\,\mathrm{d}\bar{y} = \lambda_1 \operatorname{Re}\left\{\frac{\partial^2 A}{\partial \tilde{X}^2} A^*\right\} + \lambda_2 \left|\frac{\partial A}{\partial \tilde{X}}\right|^2 + \lambda_3 \tilde{X}\bar{\kappa}_0' |A|^2, \tag{3.85}$$

where $\lambda_1, \lambda_2, \lambda_3$ are real coefficients independent of $\tilde{X}$.

Variation of $A(\tilde{X})$ now leads to the equation governing the reflection of waves. Thus

$$\tilde{\alpha}\frac{\mathrm{d}^2 A}{\mathrm{d}\tilde{X}^2} - \tilde{\beta}\bar{\kappa}_0' \tilde{X} A = 0, \tag{3.86}$$

with $\tilde{\alpha}$ and $\tilde{\beta}$ real constants which at this stage are unknown. It is not difficult, however, to determine appropriate expressions for these constants by examining the behaviour of solutions to (3.86) as we move away from the reflection point into the wave propagation region described earlier. Let us suppose that neither $\tilde{\alpha}$ or $\tilde{\beta}$ is zero. Equation (3.86) is then the Airy equation, with solution

$$A = \mathrm{Ai}\,(\tilde{\mu}\tilde{X}), \tag{3.87}$$

where

$$\tilde{\mu}^3 = (\tilde{\beta}/\tilde{\alpha})\,\bar{\kappa}_0' \tag{3.88}$$

and Ai is the Airy function. The character of the solution is as follows. As $\tilde{\mu}\tilde{X} \to +\infty$ the Airy function is exponentially decaying, representing the lack of propagating waves there. In the limit $\tilde{\mu}\tilde{X} \to -\infty$, on the other hand, we enter the wave propagation region and the asymptotic form for the solution is

$$A \sim |\tilde{X}|^{-\frac{1}{4}}(\mathrm{e}^{\mathrm{i}\theta} + \mathrm{e}^{\mathrm{i}\pi/2}\,\mathrm{e}^{-\mathrm{i}\theta}) \tag{3.89}$$

to within an arbitrary constant (Abramowitz & Stegun 1972, eq. 10.4.60). In this expansion

$$\theta = \tfrac{2}{3}|\tilde{\mu}|^{\frac{3}{2}}|\tilde{X}|^{\frac{3}{2}}. \tag{3.90}$$

Equations (3.89) and (3.90) show the wave character of the solution clearly.

The effective wavenumbers of the two components in (3.89) are given by

$$\bar{k} = \bar{k}_0 \pm |\tilde{\mu}|^{\frac{3}{2}}|X - X_0|^{\frac{1}{2}}, \tag{3.91}$$

which we may write as

$$\tilde{\alpha}(\bar{k} - \bar{k}_0)^2 + \tilde{\beta}\bar{\kappa}_0'(X - X_0) = 0. \tag{3.92}$$

Now it will be recalled that the dispersion relation for the waves is $\bar{\omega}^2 = \bar{D}(\bar{k}, \bar{\kappa})$ with $\bar{\omega}^2$ constant. At $X = X_0$ we have $\bar{\kappa} = \bar{\kappa}_0$, $\bar{k} = \bar{k}_0$ and $\partial\bar{D}/\partial\bar{k} = 0$ and so for X near X_0 Taylor's expansion gives

$$\frac{1}{2}\frac{\partial^2 \bar{D}}{\partial \bar{k}^2}(\bar{k} - \bar{k}_0)^2 + \frac{\partial \bar{D}}{\partial \bar{\kappa}}\bar{\kappa}_0'(X - X_0) = 0 \tag{3.93}$$

Comparison with (3.92) shows that

$$\tilde{\alpha} = \tfrac{1}{2}\partial^2 \bar{D}/\partial \bar{k}^2 \tag{3.94}$$

and $$\tilde{\beta} = \partial \bar{D}/\partial \bar{\kappa} \tag{3.95}$$

provide the correct value for the ratio of $\tilde{\alpha}$ and $\tilde{\beta}$. This ratio is the only significant unknown quantity in (3.86). Thus (3.94) and (3.95) determine the constants.

Special cases in which the analysis breaks down occur if $\tilde{\alpha}$ or $\tilde{\beta}$ is zero. The former case implies that the point $\bar{k}_0$ is a higher order of extremum of frequency than a simple zero of group velocity. The scalings should then be adjusted and the analysis likewise. We do not go into this case in any further depth. It was shown earlier in this section that $\tilde{\beta} = 0$ can only occur if $\bar{\kappa} = 0$ and this, together with the condition of vanishing group velocity leads to the problem considered above in §3*b*. That is, it defines the beginning of the mode sequence.

(*e*) *The higher trapped modes*

The higher trapped modes are constructed from the wave propagation and reflection problems of §3*c*, *d*. Consider a wave that crosses the point of zero curvature and propagates towards positive $\bar{x}$ with positive $\bar{k}$. The wave will undergo reflection at some point if it is to be trapped. At this point the value of $\tilde{\mu} > 0$ and it follows from (3.89) and (3.90) that the wave undergoes a phase shift of $-\frac{1}{2}\pi$ on reflection. This is in addition to the phase shift $\int \bar{k}\,\mathrm{d}\bar{x}$ which the wave has undergone in propagation. The wave now propagates towards the inflection point and may, as described in §2, undergo reflection again before reaching that point. If this occurs, the value of $\tilde{\mu} < 0$ and it again follows from (3.89) and (3.90) that the wave undergoes a phase shift of $+\frac{1}{2}\pi$ together with the propagation shift of $\int \bar{k}\,\mathrm{d}\bar{x}$ (the integral is to be taken in the sense of decreasing $\bar{x}$ as the wave propagates). Eventually the wave returns to the point of zero curvature having undergone a total phase shift equal to the sum of the propagation phase shifts and $-\frac{1}{2}\pi$. On the other side of the point of zero curvature a similar argument applies. When the wave returns to the inflection point having completed its cycle of reflections the total phase shift is

$$\oint \bar{k}\,\mathrm{d}\bar{x} - \pi. \tag{3.96}$$

To form a normal mode, the wave must arrive back in phase with its initial value. Thus for a mode,

$$\oint \bar{k}\,\mathrm{d}\bar{x} = (2n+1)\,\pi, \tag{3.97}$$

where n is an integer. We note that in dimensional terms (3.97) also reads

$$\oint k\,\mathrm{d}x = (2n+1)\,\pi \tag{3.98}$$

and that $\oint k\,\mathrm{d}x$ is the area of the curve traced out by the wave in the xk plane during its cycle of reflections. This curve is a contour of constant frequency $\omega^2 = D(k, \kappa)$ mapped into the xk plane via the functional form of κ on x.

It may be surprising that the above prescription gives the lower modal frequencies in the series accurate to the order of approximation which was used in §3*b*. This is because, as is well known in the quantum mechanical context, the WKB method gives the eigenvalues of the harmonic oscillator equation exactly, despite the fact that eigensolutions for the first few modes bear scant resemblance to the slowly varying travelling waves assumed by the method.

PHILOSOPHICAL TRANSACTIONS OF THE ROYAL SOCIETY A MATHEMATICAL, PHYSICAL & ENGINEERING SCIENCES

Figure 5

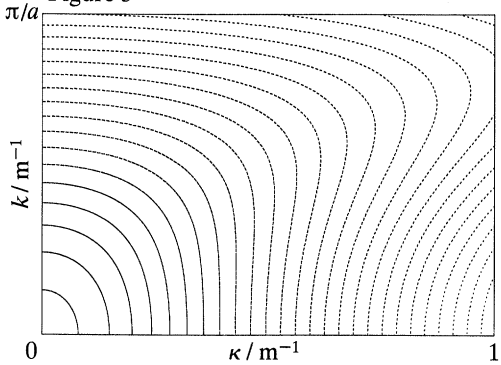

Figure 6

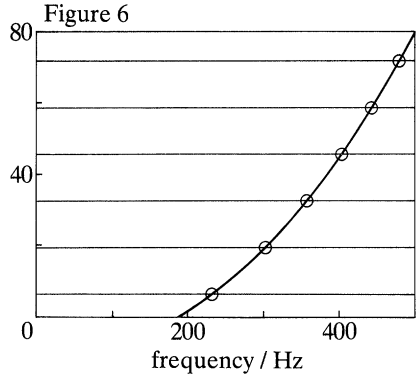

Figure 5. Lines of constant frequency in the κk plane, as explained in the text. The parameters correspond to the experimental strip of §4, and the contours are at 25 Hz intervals, starting from 200 Hz in the lower left-hand corner.

Figure 6. Plot of the left-hand side of equation (3.100) against frequency, for the parameters of the experimental strip of §4. The horizontal lines correspond to the right-hand side of equation (3.100), with a value $\eta = 2.1\ \mathrm{m}^{-2}$ corresponding to the highest curvature of the cases studied in the experiment. The ringed intersections give the predicted mode frequencies for that case.

The computations described in §2 can be used to express (3.98) in a form that makes it easy to calculate mode frequencies for any particular geometry. This will be needed to test the predictions against measured results in §4. Suppose that throughout the region of the strip within which the modes of interest are confined, the equation varies linearly with distance according to

$$\kappa = \eta x. \tag{3.99}$$

Then (3.98) becomes

$$\oint k \, \mathrm{d}\kappa = (2n+1)\,\pi/\eta. \tag{3.100}$$

If we plot the left-hand side as a function of frequency, then for any particular configuration of the strip, governed by a value of η, we have only to draw a set of lines at values $(2n+1)\,\pi/\eta$ and read off the frequencies at which they intersect the curve.

The first stage of the computation is to plot the contours of constant frequency in the $k\kappa$ plane. A typical result, for the second symmetric mode of propagation, is shown in figure 5. It is convenient to work in dimensional terms appropriate to the experiment which will be described shortly. Using the appropriate physical parameters for this strip, the cut-on frequency for the second symmetric mode on the flat strip is 188 Hz, so the contours of constant frequency were chosen to start at 200 Hz (in the lower left-hand corner) and rise in steps of 25 Hz. Curvature is plotted along the x axis, from zero to a maximum corresponding to a radius of curvature of 1 m. Wavenumber is plotted on the y axis, from zero up to a value corresponding to a wavelength equal to twice the width of the strip.

The shapes of the contours fall into two classes, corresponding to the two shapes seen in the dispersion curves of figure 3. Near the origin of the $k\kappa$ plane the contours are convex, corresponding to the monotonic dispersion curves for low curvature. Further out the curves cease to be convex, corresponding to the dispersion curves which fall and then rise.

To calculate $\oint k \, \mathrm{d}\kappa$, we simply compute the area inside the closed loop contour for a given frequency, allowing of course for the other three quadrants of the $k\kappa$ plane,

PHILOSOPHICAL TRANSACTIONS OF THE ROYAL SOCIETY A MATHEMATICAL, PHYSICAL & ENGINEERING SCIENCES

which are simply mirror images of the quadrant plotted in figure 5. The resulting curve is plotted in figure 6. It starts from the cut-on frequency, with an initial gradient which is responsible for the mode spacing for low modes given in (3.57).

Superimposed on the curve is a set of horizontal lines corresponding to $(2n+1)\,\pi/\eta$ for one of the cases of the experimental measurements to be described shortly. The intersections, shown ringed, give the predicted mode frequencies for this case. Notice that the mode-spacing behaviour is quite different from that near a normal waveguide cut-on. Usually, a cut-on corresponds to a zero value of group velocity, and the mode spacing tends to zero at cut-on. It then increases as frequency rises. In this problem, by contrast, the mode spacing is greatest for the lowest modes, and decreases for higher frequencies. The difference arises from the fact that the confinement length-scale increases with mode number for this problem, whereas one is more used to problems in which all modes are confined between fixed ends.

4. Experimental results on trapped modes

An experiment was carried out to test the theoretical predictions of §3. A strip of mild steel 1011 mm × 153 mm × 0.795 mm was used for the testpiece. Its density was measured to be 7770 kg m^{-3}. This strip was held in a variety of S-shaped configurations, and the first few frequencies of confined modes based on the second symmetric waveguide branch were observed. Some information was also obtained about the axial variation of the corresponding mode shapes. From a knowledge of the material properties of the steel strip and the geometric parameters describing a given configuration, a set of frequencies could be calculated from (3.100) for comparison with the measured results in each case.

For each configuration of the strip the value of η must be determined. This involves testing the validity of the assumption of linear variation, (3.99), and measuring the rate of change of curvature with distance. It proved difficult to determine the curvature profile with sufficient accuracy from simple geometric measurement, so a system of strain gauges was used for this purpose. Seven pairs of gauges were fixed at 100 mm intervals along the centre line of the strip, symmetrically placed about the centre point. The gauges of each pair were on opposite faces of the strip, aligned axially along the strip. By connecting each pair of gauges in an appropriate bridge circuit to respond only to deformations antisymmetric about the central surface of the strip, a steady reading could be obtained which was proportional to the curvature at the relevant point on the saw, while the fluctuating part of the same signals, following impulsive excitation of the strip, could be used for measurement of bending vibrations.

The nominal calibration of the gauges was checked, and simultaneously the Young's modulus of the strip determined accurately, by observing the signals resulting from the deformation of the strip under its own weight when held on two symmetrically placed point supports. This was achieved by laying the strip across a pair of steel rollers supported on a flat surface. By varying the spacing of the rollers, a variety of different shapes of deformation can be achieved. The usual small-displacement theory of bending beams yields a very simple expression for this displacement in any given case, and hence for the curvature profile with distance along the strip.

For several different spacings of the rollers the set of voltages from the strain-gauge bridges was recorded, and in each case the centre-point displacement of the

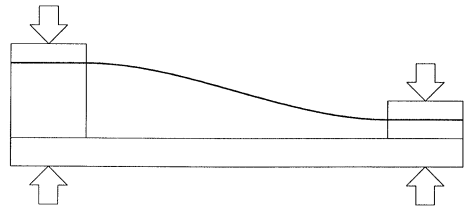

Figure 7. Sketch of the experimental arrangement for holding the strip in an S-shaped configuration. Clamps were applied at the two pairs of arrows.

strip was also measured directly. For each roller position the strip was measured both ways up, to compensate for any permanent deformation that might bias the results. In each case the curvature profile was in good agreement with the theoretical results. From these results Young's modulus was determined to be 210 GPa. Poisson's ratio was taken to be 0.28. The set of calibration factors and physical parameters was thus complete.

The next stage was to hold the strip in an S-shaped configuration complying with the assumptions of the theory. This required that curvature should vary linearly with distance along the strip, and that there should be no axial tension or compression in the strip, since this would add extra terms to the potential energy which would shift the mode frequencies. It was desired to achieve values of η over a reasonable range, to test the predictions thoroughly.

Two methods were used for holding the strip in a suitable shape. First, it was clamped to a rigid board with an asymmetric arrangement of blocks as illustrated in figure 7. All generators of the strip were vertical, to eliminate any self-weight distortion. The aim was to apply equal and opposite end moments but no end forces to the strip, since under those conditions standard beam theory predicts precisely the linear variation of curvature which we require. With the clamping arrangement, it proved quite difficult to avoid axial forces as the clamps were tightened, especially for the more extreme cases of curvature. But the method worked quite well with low curvature, and had the advantage of holding the strip in a stable shape for an indefinite period so that repeated measurements could be taken.

The second method used was to hold the strip by hand, in much the way that a player of the musical saw holds their instrument. It proved quite easy to achieve an accurate linear variation of curvature by this method, especially with higher values of curvature. It would appear that we are able to feel, and thus avoid, axial forces of sufficient magnitude to disturb the behaviour here being studied. The disadvantage of hand holding, of course, is that one cannot guarantee to hold the shape completely steady for an extended period of time. Thus it was possible to record single sets of data from all seven sensors following impulsive excitation of the strip, but it was not possible to obtain repeated measurements under identical conditions.

We present results for four different configurations of the strip. Of these, the first two were clamped while the second two were hand-held. Plots of measured curvature at the seven gauge positions for each configuration are shown in figure 8. For the two clamped cases, figure 8*a*, *b*, we see that the curvature varies with reasonable linearity along the strip, except for the final sensor position in each case. This deviation from linearity at one end appeared to arise from slight permanent deformation of the strip near the end, in the form of curvature across the width. It does not influence modes that are confined near the strip centre. In each figure a straight line is also plotted, which represents a regression fit to the six points for which good linear variation is

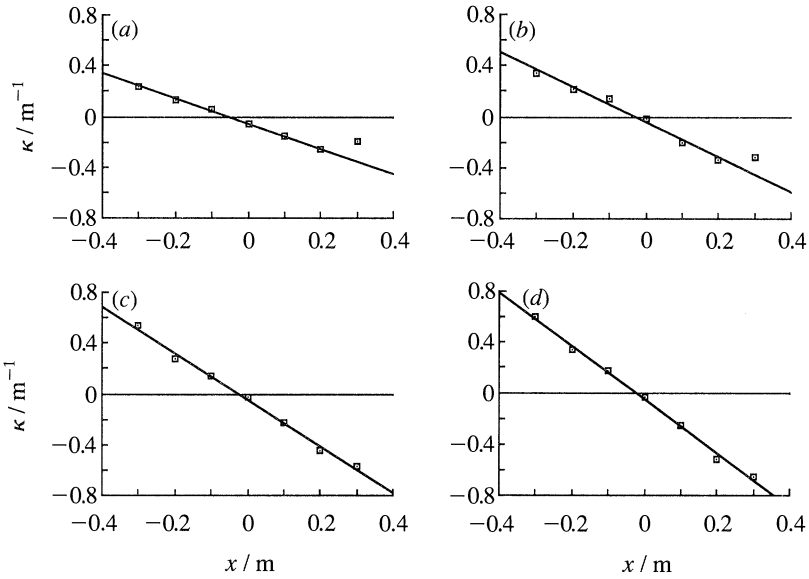

Figure 8. Plots of measured curvature against distance along the strip for the four cases studied, together with the regression lines for determining η in each case.

observed. For the two remaining cases, figure 8*c*, *d*, based on hand-held strip configurations, good linearity is seen across all seven sensor sites, and the regression fit is based on all the points in these cases.

From the four regression fits, we can deduce the values of η required for the theoretical prediction of confined-mode frequencies. These were 0.98, 1.4, 1.8 and 2.1 m^{-2} respectively for the four cases. This gives a range rather greater than a factor of two, which is sufficient for a thorough check of the theory. Notice from figure 8 that the points of zero curvature do not fall exactly on the central gauge. Instead there is an offset, determined by the detailed end conditions in each case, which can be determined from the intercept of each regression line. These offsets must be taken into account when interpreting the mode shape measurements.

Vibration signals were obtained in each case by tapping the strip at a point on its centre line and collecting the seven channels of strain gauge data simultaneously in a digital data-logger. This gave the large dynamic range necessary to cope with rather small fluctuating signals superimposed on large steady levels representing the mean curvature profile. Fourier analysis then yielded a vibration spectrum for each gauge position. The peaks in these spectra give mode frequencies, while the variation with position of the spectral amplitude and phase gives information about the corresponding mode shape associated with a given peak. With our rather sparse gauge spacing, the mode-shape information does not have very good spatial resolution. However, it allows the predicted shapes of the successive modes to be checked quite adequately.

Because the strain gauges were placed on the strip centre-line, we only observe the waveguide modes that are symmetric, in other words the ones allowed for in the computations of figure 3. We thus expect to see confined modes based on the second symmetric mode, together with some effects of the lowest, bending-beam, mode. These latter modes are not confined by the mechanism under study, but nevertheless there will be modes based on boundary reflection of the usual sort. These turn out to

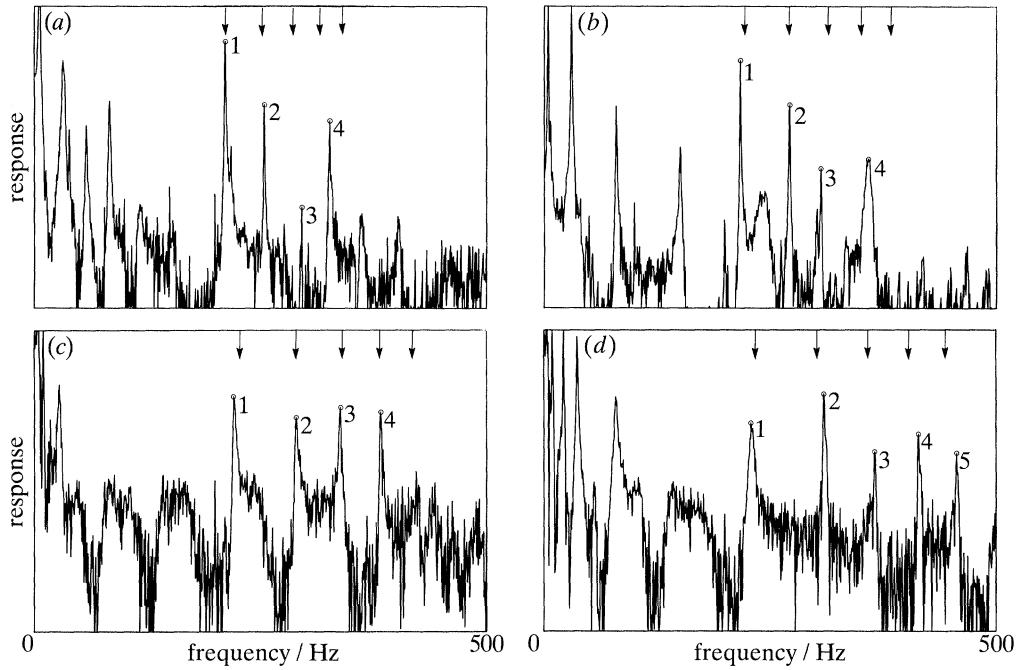

Figure 9. Measured frequency spectra following impulsive excitation of the strip in the four different curvature configurations. In all cases, the frequency scale is linear from zero to 500 Hz, while the vertical scale is logarithmic with a total range of 40 dB. Case (*a*) $\eta = 0.98\ \mathrm{m}^{-2}$; case (*b*) $\eta = 1.4\ \mathrm{m}^{-2}$; case (*c*) $\eta = 1.8\ \mathrm{m}^{-2}$; case (*d*) $\eta = 2.1\ \mathrm{m}^{-2}$. Ringed and numbered peaks are the confined modes under study, arrows at the top of each figure show the predicted frequencies according to (3.100).

be much more prominent in the experimental results when the strip is clamped between blocks, and less so when hand-held. The reason, no doubt, is that despite efforts to add boundary damping in the clamping rig by using foam, the human finger proves a more effective damper of non-confined modes.

A representative spectrum from each configuration is plotted in figure 9*a–d*. In each case, the frequency scale is linear from zero to 500 Hz, while the amplitude scale is logarithmic with a total range of 40 dB. The predicted frequencies of the first few confined modes, based on the second symmetric waveguide mode according to the theory given earlier, are indicated on each spectrum by arrow markers along the top edge of the graph. Those on figure 9*d*, for the highest value of η, are taken directly from figure 6. The other cases are calculated from the same graph, but using appropriately different spacings of the set of horizontal lines for each value of η.

In each spectrum, the set of peaks that are to be compared with the predictions are marked with rings and numbered. In figure 9*a*, for the case with lowest curvature, we see a good match with the first two confined modes, but by the time we reach the modes labelled 3 (which happens to have a node line close to our excitation position) and 4 the frequencies are not very well predicted, the observed frequencies being higher than the predicted ones. This is not a failure of the theory : with this low value of curvature, only the first two modes are predicted to have a confinement length-scale that is shorter than the length of strip between the clamping blocks. The higher modes are reaching the ends of the strip, and boundary reflection then takes over

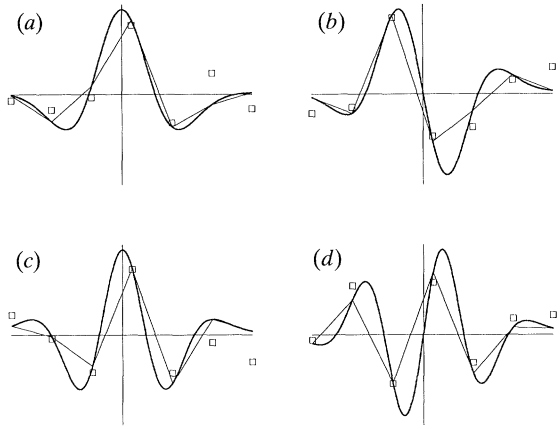

Figure 10. The first four confined modes for the second symmetric waveguide branch, for the configuration with $\eta = 2.1\ \mathrm{m}^{-2}$. Heavy lines: shapes according to (3.58); fine lines: theoretical values at the points corresponding to the sensor positions; square symbols: experimental values. The variable plotted is the second spatial derivative of the modal displacement.

from internal reflection as the process governing mode frequencies. Since the free length of strip is too short for the predicted confined modes, it is to be expected that the frequencies will be higher than predicted.

In figure 9*b*, with somewhat greater curvature, we see a reasonable match to the first three confined-mode frequencies. All are a little lower than the predictions, which may be the result of slight axial compression in the strip. This time, mode 4 is the one which reaches the ends, and so has a higher frequency than that predicted by the confined-mode theory. Figure 9*c*, *d* show the higher-curvature hand-held cases. Figure 9*c* shows good agreement of frequencies for the first four modes. Figure 9*d* shows five confined modes, although in this case the agreement with predicted frequencies is rather less precise. The reason for this slight disagreement is not clear, but it does not seem sufficiently serious to cast doubt on the essential correctness of the theoretical account of mode confinement given above.

Finally, we look at some results for mode shapes. Approximate values of modal amplitudes at the sensor positions have been obtained by the simplest procedure, and this proves adequate to show good agreement with the theory. The modes of interest produce very precisely defined resonance peaks. From any particular set of data, peak amplitudes and phases from the different sensor channels mirror the spatial variation of the mode in question, provided the peak values rise well above the background level produced by the other modes. Thus the amplitudes, with signs deduced from the phase behaviour, give a direct indication of the mode shape, at least for the points where the modal amplitude is large. We can expect significant errors where signal is small, either because the measurement point falls close to a node line or because we are near the ends of the strip so that the confinement effect produces small amplitudes.

Mode shapes were examined for all the labelled peaks in figure 9. It is sufficient to show here one set of modes, and we have chosen the set corresponding to the most curved case, from figure 9*d*. Figure 10 shows the first four mode shapes. Note that the quantity plotted is not displacement: the measurements are of curvature rather than displacement, so the correct quantity to compare with the experimental values is the second derivative of the displacement mode shape with respect to axial

PHILOSOPHICAL TRANSACTIONS OF THE ROYAL SOCIETY A MATHEMATICAL, PHYSICAL & ENGINEERING SCIENCES

distance x, the modal curvature profile. In each case, then, the smooth curve is the predicted curvature deduced from (3.58) and (3.59). The zig-zag line highlights the particular values on each theoretical curve which correspond to the sensor sites (allowing for the offset of the zero point of curvature deduced from figure 8*d*). The experimental amplitudes, with a suitably chosen overall scale factor, appear as the plotted square symbols.

The agreement between theory and experiment is excellent for all four modes, at least for the points near the centre where the predicted amplitudes are large so that the rather crude method of deducing mode shapes from the measured data is adequate. Where the expected signal is smaller, a more sophisticated technique of experimental modal analysis would be needed. The mode shapes are alternately symmetric and antisymmetric in their axial variation, with respect to the point of zero curvature. The offset of this point from the central sensor position makes this alternation not immediately apparent in the experimental results, but with the zig-zag line to mark the relevant points for comparison the correspondence is clear. Bearing in mind that this case was the one for which the frequencies were predicted least accurately, these results seem entirely satisfactory.

5. The bending-beam modes

(*a*) *Experimental results*

We now turn to a discussion of the modes based on the lowest symmetric waveguide branch, 'bending-beam' modes. Although not confined by the process of internal reflection described in previous sections, these modes do show an interesting effect of curvature. Up to now, the branches have been classified according to symmetry of the normal motion with respect to the centre line of the strip, i.e. symmetry under reflection *across* the strip. The lowest branch is always symmetric in this sense. In this section we shall also be concerned with symmetry properties of modes, but here the important symmetry relates to the behaviour under reflection *along* the strip about the middle of the S. (We suppose the strip geometry to be symmetric about the middle of the S.)

The modal analysis described in §4 can also be applied to the peaks at low frequency, corresponding to non-confined modes based on the bending-beam branch. Figure 11 shows the first seven of these modes, for one of the cases in which the strip was held in the S-shaped configuration by clamping. (Recall that what is plotted is not displacement but curvature in the modal configurations.)

This figure reveals an unexpected phenomenon. In most symmetric systems the mode sequence consists of alternating axially symmetric (s) and axially anti-symmetric (a) modes: the sequence runs a/s/a/s/a, where the modes are ordered in frequency. The sequence revealed here runs s/s/a/a/s/a/s. The second and third modes in the sequence appear in the reverse order to what one would anticipate. Investigation of this phenomenon is the subject of this section.

(*b*) *Analysis*

We use the non-dimensional shell theory described previously, and assume that vibrational displacement is uniform across the strip, so that

$$\bar{u}_x = U(\bar{x}), \tag{5.1}$$

$$\bar{u}_y = 0 \tag{5.2}$$

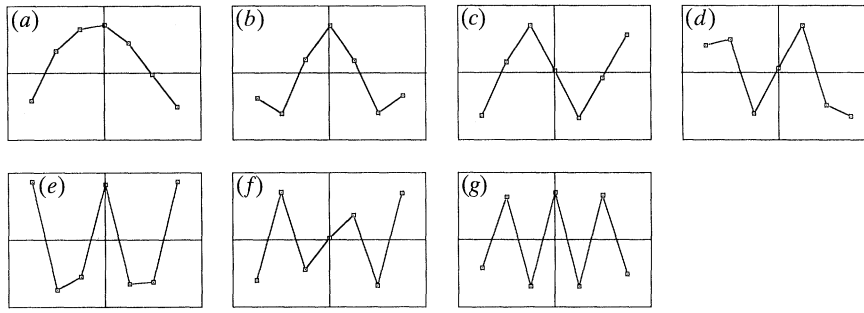

Figure 11. The first seven mode shapes measured from the experimental strip, with $\eta = 1.4\ \mathrm{m}^{-2}$. The symbols give the individual sensor results, and the lines connecting them are purely a guide for the eye. Second spatial derivative of modal displacement is plotted against axial position along the strip centre-line. (*a*) Mode 1, 4.9 Hz; (*b*) mode 2, 30.5 Hz; (*c*) mode 3, 45.2 Hz; (*d*) mode 4, 65.3 Hz; (*e*) mode 5, 80 Hz; (*f*) mode 6, 116.6 Hz; (*g*) mode 7, 150.8 Hz.

and
$$\bar{w} = W(\bar{x}), \tag{5.3}$$

where $-\frac{1}{2}\bar{l} < \bar{x} < \frac{1}{2}\bar{l}$ gives non-dimensional position along the strip, these limits being the ends of the strip.

The assumed form (5.1)–(5.3) is not a solution of the shell equations and boundary conditions unless Poisson's ratio, $\sigma = 0$. However, we may regard the forms (5.1)–(5.3) as trial functions in the sense of Rayleigh's principle, which become exact when $\sigma = 0$. Computed results for strips of constant curvature indicate that the motion for a steel strip is well approximated by this form.

Substituting into the non-dimensional lagrangian density given earlier yields

$$\bar{L} = \left(\frac{\mathrm{d}U}{\mathrm{d}\bar{x}} - \bar{\kappa}W\right)^2 + \left(\frac{\mathrm{d}^2W}{\mathrm{d}\bar{x}^2}\right)^2 - \bar{\omega}^2W^2. \tag{5.4}$$

The first term in (5.4) corresponds to extension of the strip, the second to bending, and the last to inertia. Applying the variational principle

$$\delta \int_{-\frac{1}{2}\bar{l}}^{\frac{1}{2}\bar{l}} \bar{L}\,\mathrm{d}\bar{x} = 0 \tag{5.5}$$

yields the equations of motion for the strip:

$$\frac{\mathrm{d}}{\mathrm{d}\bar{x}}\left(\frac{\mathrm{d}U}{\mathrm{d}\bar{x}} - \bar{\kappa}W\right) = 0 \tag{5.6}$$

and
$$\frac{\mathrm{d}^4W}{\mathrm{d}\bar{x}^4} - \bar{\omega}^2W = \bar{\kappa}\left(\frac{\mathrm{d}U}{\mathrm{d}\bar{x}} - \bar{\kappa}W\right). \tag{5.7}$$

According to (5.6)
$$\frac{\mathrm{d}U}{\mathrm{d}\bar{x}} - \bar{\kappa}W = \tau, \tag{5.8}$$

where τ is constant. This equation expresses the condition that the mean axial tension in the strip is independent of $\bar{x}$, a requirement arising from in-surface equilibrium. Using (5.8) in (5.7) gives

$$\frac{\mathrm{d}^4W}{\mathrm{d}\bar{x}^4} - \bar{\omega}^2W = \bar{\kappa}\tau, \tag{5.9}$$

which is the usual bending beam equation with an additional term, $\bar{\kappa}\tau$, representing curvature and tension.

The boundary conditions at the ends of the strip ($\bar{x} = \pm\frac{1}{2}\bar{l}$) enter as constraints on the variational problem (5.5) arising from Hamilton's principle. We consider three cases:

(i) *Free ends*

These result in no constraints.

(ii) *Hinged ends*

$$U = W = 0. \tag{5.10}$$

(iii) *Clamped ends*

$$U = W = \mathrm{d}W/\mathrm{d}\bar{x} = 0. \tag{5.11}$$

The corresponding boundary conditions arising from the variational principle are then

(i) $$\tau = \mathrm{d}^2W/\mathrm{d}\bar{x}^2 = \mathrm{d}^3W/\mathrm{d}\bar{x}^3 = 0, \tag{5.12}$$

(ii) $$U = W = \mathrm{d}^2W/\mathrm{d}\bar{x}^2 = 0, \tag{5.13}$$

(iii) $$U = W = \mathrm{d}W/\mathrm{d}\bar{x} = 0, \tag{5.14}$$

at the ends, which supplement (5.8) and (5.9) and complete the specification of the problem for the normal modes. Note that when either end of the strip is free, $\tau = 0$ and these equations become the usual bending beam equation, with the usual boundary conditions. The curvature is then unimportant because of the lack of mean axial tension.

We do not consider cases where there are different boundary conditions at the two ends. Thus cases (i), (ii) and (iii) describe free–free, hinged–hinged and clamped–clamped strips respectively. For the free–free case the resulting modes do not depend on curvature and can be classified as either symmetric or antisymmetric about $\bar{x} = 0$. The resulting modal frequencies are given by $\bar{\omega} = 4\nu^2/\bar{l}^2$, where ν^2 is a non-dimensional frequency occurring naturally throughout our analysis. For the free–free strip ν satisfies the transcendental equations $\tan\nu \pm \tan h\nu = 0$ (see, for example, Rayleigh 1894), where the + sign refers to modes symmetric in $\bar{x}$ and the − sign gives the antisymmetric modal frequencies. The positive roots of the above equations are used later in this section and we denote them by $\nu_n^{(\pm)}$ ($n = 1, 2, \ldots$). They are ordered so that $\nu_n^{(\pm)}$ increases with increasing n. These free–free roots $\nu_n^{(\pm)}$, and consequently the modal frequencies in case (i), are interlaced: the lowest is a symmetric mode ($\nu_1^{(+)}$) the next an antisymmetric one ($\nu_1^{(-)}$), followed by $\nu_2^{(+)}$ (symmetric), then $\nu_2^{(-)}$ (antisymmetric), and so on.

For future reference, note that dimensional frequency can be obtained from ν via

$$\omega = \left[\frac{Eh^2}{12(1-\sigma^2)\rho}\right]^{\frac{1}{2}} \frac{4\nu^2}{l^2}, \tag{5.15}$$

where as before E, ρ and σ are the Young's modulus, density and Poisson's ratio of the strip material, h is the thickness of the strip and l its length. This equation shows explicitly that ν^2 is a non-dimensional frequency.

Before analysing the hinged–hinged and clamped–clamped problems with curvature, we briefly consider the corresponding results for a flat strip. We again

recover classical beam problems. The hinged–hinged problem, (ii), yields $\nu = (n-\frac{1}{2})\pi$ $(n = 1, 2, \ldots)$ for the symmetric modes and $\nu = n\pi$ $(n = 1, 2, \ldots)$ for the antisymmetric modes. The clamped–clamped problem, (iii), has the same modal frequencies as the free–free one considered above, namely $\nu_n^{(\pm)}$, apart from rigid-body modes with zero frequency (because the second spatial derivative of a free–free eigenfunction is a clamped–clamped eigenfunction).

With curvature, in either of cases (ii) or (iii) we have $U = 0$ at the ends. Thus (5.8) yields

$$\bar{l}\tau = -\int_{-\frac{1}{2}\bar{l}}^{\frac{1}{2}\bar{l}} \bar{\kappa} W \, \mathrm{d}\bar{x}, \tag{5.16}$$

while (5.9) can be written

$$\frac{\mathrm{d}^4 W}{\mathrm{d}\bar{x}^4} - \frac{16\nu^4}{\bar{l}^4} W = \bar{\kappa}\tau \tag{5.17}$$

and the boundary conditions at the ends are

(ii) $$W = W'' = 0 \tag{5.18}$$

or

(iii) $$W = W' = 0. \tag{5.19}$$

Equations (5.16)–(5.19) define the problem with curvature.

For general $\bar{\kappa}(\bar{x})$ the solution of (5.16)–(5.19) is not straightforward, but for the particular case of a strip bent into an ideal S-shape things are made tractable by the fact that the curvature, $\bar{\kappa}$, is a linear function of $\bar{x}$. We shall henceforth assume this to be the case. We shall also suppose that the centre of the S-shape (where $\bar{\kappa} = 0$) lies at the centre of the strip so that $\bar{\kappa} = \bar{\eta}\bar{x}$. The fact that $\bar{\kappa}$ is then an odd function of $\bar{x}$ means that the strip is symmetric about $\bar{x} = 0$ and the modes divide into those which are symmetric and antisymmetric about $\bar{x} = 0$, as for a flat strip.

For the symmetric modes, (5.16) yields $\tau = 0$, and we recover the classical beam problems without curvature. This is because such symmetric vibrations do not cause any net extension of the strip. The modal frequencies are again determined by

(ii) $$\nu = (n-\tfrac{1}{2})\pi$$

or

(iii) $$\nu = \nu_n^{(+)}$$

as if the strip were flat. We may note that if $\bar{\kappa}(\bar{x})$ were an *even* function of $\bar{x}$ the strip would again be symmetric (in a slightly different sense) and that again the modes would divide according to symmetry. However, it would then be the *antisymmetric* modes which would be unaffected by curvature while the symmetric ones were altered. We do not pursue this case further, but note that it would show similar behaviour in terms of unexpected ordering of symmetric and antisymmetric modes: one class of modes is raised in frequency by curvature while the other class is left unchanged, so that a failure of strict interleaving, referred to above, occurs. In our case, it is the symmetric modes that remain the same and the antisymmetric modes that are raised in frequency.

For the antisymmetric modes with $\bar{\kappa} = \bar{\eta}\bar{x}$, the problem (5.16)–(5.19) can be solved, leading to the equations

(ii) $$\frac{\nu^4}{\zeta^2} = 1 - \frac{3(\coth\nu - \cot\nu)}{2\nu} \tag{5.20}$$

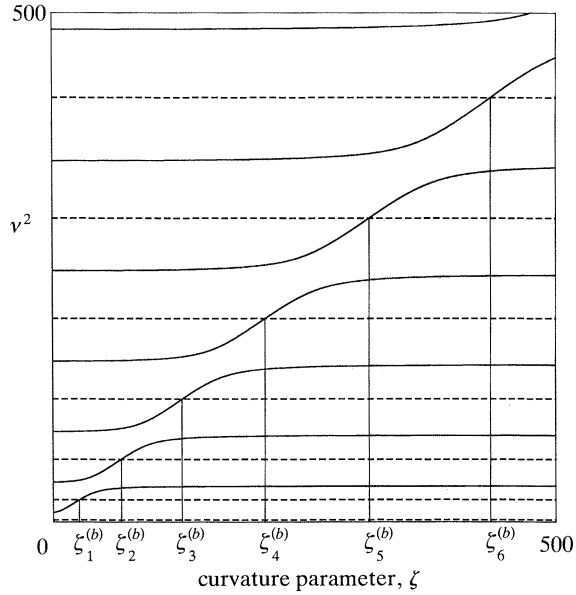

Figure 12. Frequency parameter ν^2 plotted against curvature parameter ζ for hinged end conditions. Symmetric modes appear as (horizontal) dashed lines, while antisymmetric modes appear as solid lines.

Table 2.

	symmetric	antisymmetric
free–free	$\nu_n^{(+)}$	$\nu_n^{(-)}$
hinged–hinged	$(n-\frac{1}{2})\pi$	$\nu_n^{(b)}(\zeta)$
clamped–clamped	$\nu_n^{(+)}$	$\nu_n^{(c)}(\zeta)$

and

(iii) $$\frac{\nu^4}{\zeta^2} = 1 - \frac{6(\nu - \tanh\nu)(\tan\nu - \nu)}{\nu^3(\tan\nu - \tanh\nu)} \tag{5.21}$$

respectively for the two cases, where $\zeta = \bar{\eta}\bar{l}^3/8\sqrt{3}$ is a measure of curvature which can be written in terms of dimensional quantities as

$$\zeta = l^3\eta/4h. \tag{5.22}$$

We denote the ordered sets of positive roots of (5.20) and (5.21) by $\nu_n^{(b)}(\zeta)$ and $\nu_n^{(c)}(\zeta)$ $(n = 1, 2, \ldots)$. Table 2 summarizes the notation and results obtained so far.

We now consider the antisymmetric modes in more detail, for cases (ii) and (iii). Each of equations (5.20) and (5.21) has the form

$$\nu^4/\zeta^2 = F(\nu). \tag{5.23}$$

In either case $F(0) = 0$ and F is a decreasing function of ν between recurring infinities. As curvature, represented by ζ, increases from zero to infinity, the roots, $\nu_n^{(b)}(\zeta)$ and $\nu_n^{(c)}(\zeta)$, increase from their flat-plate values, $n\pi$ and $\nu_n^{(-)}$ respectively, to limiting values $\nu_n^{(b)}(\infty)$ and $\nu_n^{(c)}(\infty)$, which are zeros of $F(\nu)$.

Figures 12 and 13 show plots of the non-dimensional frequencies $\nu_n^{(b)}(\zeta)^2$ and $\nu_n^{(c)}(\zeta)^2$ against the curvature parameter ζ. These are the central results of this section and

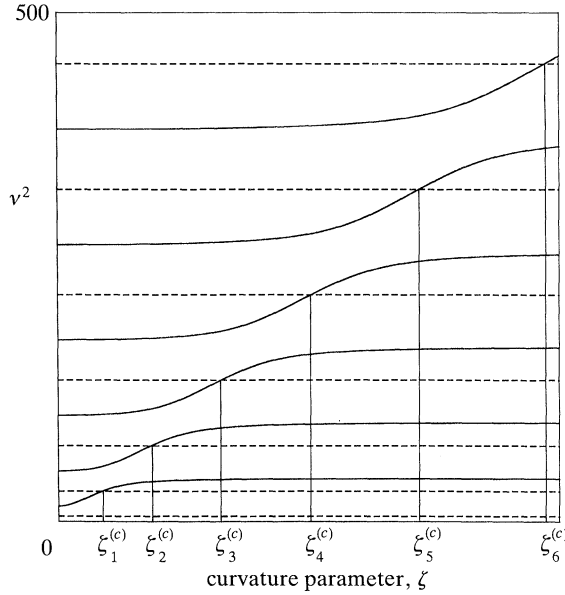

Figure 13. Frequency parameter ν^2 plotted against curvature parameter ζ for clamped end conditions. Symmetric modes appear as (horizontal) dashed lines, while antisymmetric modes appear as solid lines.

show how the frequencies of the antisymmetric modes are affected by curvature. The non-dimensional frequencies of the corresponding symmetric modes are also shown as dashed lines, which are horizontal since they are uninfluenced by curvature.

We see clearly in these figures the effect noted above, that as curvature goes to infinity ($\zeta \to \infty$) each modal frequency tends to a definite limiting value independent of curvature. In this limit the curvature is so large that any normal motion, W, of the strip would induce unacceptably large extensions of the strip unless

$$\int_{-\frac{1}{2}\bar{l}}^{\frac{1}{2}\bar{l}} \bar{\kappa} W \, \mathrm{d}\bar{x} = 0 \tag{5.24}$$

which together with (5.17) can be used to derive $\nu_n^{(b)}(\infty)$ and $\nu_n^{(c)}(\infty)$.

An alternative approach to this limit, which may have more physical appeal, is to adopt inextensionality of a highly curved strip from the start. In this approach, we drop the extensional term from (5.4) to give the lagrangian density for a flat strip

$$\bar{L} = (\mathrm{d}^2 W/\mathrm{d}\bar{x}^2)^2 - \bar{\omega}^2 W^2 \tag{5.25}$$

and adopt (5.24) as an inextensional constraint on the variational principle. This method leads to the same result as the above analysis in the infinite curvature limit. (The quantity τ then appears as a Lagrange multiplier.)

Observe that, no matter how large ζ may be, sufficiently high in the mode series the frequencies approach those of a flat strip. Curvature affects the lowest mode first, and increasing ζ causes higher and higher antisymmetric modes to be raised in frequency. When we consider the ordering of the total series of modes, both symmetric and antisymmetric, the first symmetric mode is always the lowest. For $\zeta < \zeta_1^{(b/c)}$, the conventional interleaving of symmetric and antisymmetric modes applies. However, for larger curvatures ($\zeta > \zeta_1^{(b/c)}$) the first antisymmetric mode is

Table 3. *Values of ν and $\zeta_n^{(b)}$ for a hinged–hinged strip*

symmetric		antisymmetric		
n	$(n-\frac{1}{2})\pi$	$n\pi$ $(\zeta=0)$	$\nu_n^{(b)}(\infty)$ $(\zeta=\infty)$	$\zeta_n^{(b)}$
1	1.57	3.14	5.96	26.90
2	4.71	6.28	9.23	68.58
3	7.85	9.43	12.43	130.10
4	11.00	12.57	15.60	211.39
5	14.14	15.71	18.76	312.42

Table 4. *Values of ν and $\zeta_n^{(c)}$ for a clamped–clamped strip*

symmetric		antisymmetric		
n	$\nu_n^{(+)}$	$\nu_n^{(-)}$ $(\zeta=0)$	$\nu_n^{(c)}(\infty)$ $(\zeta=\infty)$	$\zeta_n^{(c)}$
1	2.37	3.93	6.53	43.98
2	5.50	7.07	9.87	92.06
3	8.64	10.21	13.10	160.56
4	11.78	13.35	16.30	248.99
5	14.92	16.49	19.47	357.22

raised in frequency above the second symmetric mode. The modal ordering as a function of frequency therefore begins s/s/a/a/s. When ζ further increases above $\zeta_2^{(b/c)}$, the second antisymmetric mode frequency passes that of the third symmetric mode and the mode sequence begins s/s/a/s/a/a.

In general, when $\zeta_n^{(b/c)} < \zeta < \zeta_{n+1}^{(b/c)}$, the mode sequence begins s/s/a and continues with alternate symmetric and antisymmetric modes, apart from a pair of antisymmetric modes which are consecutive. This pair of antisymmetric modes are the $(2n+1)$th and $(2n+2)$th of the total mode sequence and restore conventional behaviour for higher modes. Tables 3 and 4 give numerical values for the first few modes. Table 3 applies to a hinged–hinged strip and table 4 to a clamped–clamped one. The values of ν for a free–free strip ($\nu_n^{\pm}$) can also be obtained from table 4.

The qualitative behaviour shown in both figures 12 and 13 is similar. The essential physics behind this behaviour may be revealed by a simple argument. We first note that the normal component of the mode *shape* does not go through any especially significant transformation when ζ passes through the range in which that particular mode's frequency is affected. For the case of clamped boundaries, for example, the normal motion $W(\bar{x})$ corresponding to the eigenvalue equation (5.21) may be written

$$W \propto -(2\nu\bar{x}/\bar{l})\,[\sin\nu - \cos\nu\tanh\nu] + (\nu - \tanh\nu)\sin(2\nu\bar{x}/\bar{l}) + (\tan\nu - \nu)\,(\cos\nu/\cosh\nu)\sinh(2\nu\bar{x}/\bar{l}). \quad (5.26)$$

The proportionality sign merely indicates that no particular normalization has been applied to this expression. Notice that this expression does not depend explicitly on curvature ζ, but only on the dimensionless frequency ν. There is a continuum of possible shapes satisfying the equation (5.17) and the boundary conditions (5.19), and the discrete values of frequency are selected by the need to satisfy the constraint (5.16). As ν varies with curvature, the mode shape follows. This family of shapes is illustrated in figure 14. This shows how the expression (5.26) changes as ν varies

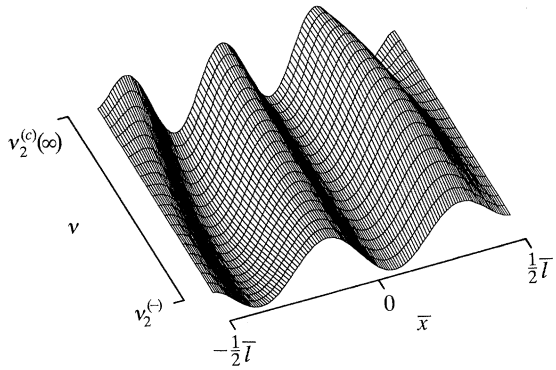

Figure 14. The dependence of axial mode shape on frequency parameter ν for the second axially antisymmetric mode.

linearly from $\nu_2^{(-)}$ to $\nu_2^{(c)}(\infty)$, the whole range of variation of the second antisymmetric mode. The overall antisymmetric nature of this mode is evident, as is the evanescent field near both ends to satisfy the clamped conditions. But apart from this, little is occurring except the gradual increase in wavenumber as ν increases.

To understand the physics, then, we must understand the eigenvalue equation. This is most easily done by considering large ν (although the conclusions hold qualitatively for all ν). In that case, the second term on the right-hand sides of both equations (5.20) and (5.21) is very small unless we are near a root of $\tan\nu = 0$ in the case of (5.20), or of $\tan\nu = \tanh\nu$ in the case of (5.21). It follows that away from the line $\nu^2 = \zeta$ the modal frequencies are approximately those of a strip without curvature. This is true even in the limit $\zeta \to \infty$, so that for high modal frequency the set of infinite-curvature limiting frequencies is approximately the same as the set of zero-curvature frequencies. As a given flat-strip mode frequency is raised by increasing curvature, it moves up to the approximate frequency of the next flat-strip mode.

To understand the behaviour near the line $\nu^2 = \zeta$ we refer back to equations (5.16)–(5.19). The solution of (5.17) has the form

$$W = -\frac{\bar{l}^4\bar{\kappa}\tau}{16\nu^4} + W_0, \tag{5.27}$$

where W_0 consists of terms which are either proportional to $\sin 2\nu\bar{x}/\bar{l}$ and therefore rapidly oscillatory, or are exponentially small away from the ends of the strip. (This form for W looks somewhat different from the explicit expression for the clamped case, equation (5.26), because of a different choice of overall multiplying factor. The first term of (5.26), linear in $\bar{x}$, corresponds to the first term in (5.27), while the term W_0 in (5.27) contains the second and third terms of (5.26).)

Using (5.27) in (5.16) we obtain

$$\bar{l}\tau\left[1 - \frac{\zeta^2}{\nu^4}\right] = -\int_{-\frac{1}{2}\bar{l}}^{\frac{1}{2}\bar{l}} \bar{\kappa} W_0 \, \mathrm{d}\bar{x} \tag{5.28}$$

and we may argue that τ is generally small owing to the oscillatory/evanescent behaviour of W_0 when ν is large, but becomes larger near the line $\nu^2 = \zeta$ owing to the factor $[1 - \zeta^2/\nu^4]^{-1}$ which occurs when we solve (5.28) for τ. We have already seen that the modes are those of a flat strip when ν is large, away from the line $\nu^2 = \zeta$. Thus

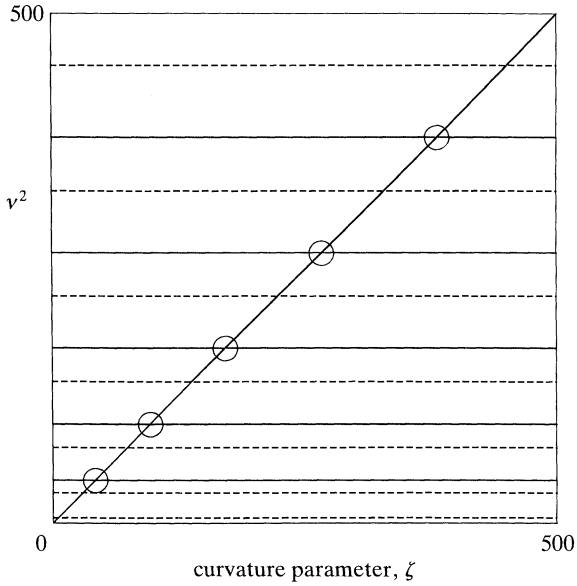

Figure 15. An interpretation of figure 13 in terms of two separate approximate theories. The horizontal lines show frequencies for the constrained (infinite-curvature) clamped strip, while the sloping line is the prediction of membrane shell theory. At the ringed intersections strong coupling occurs, invalidating the approximations of these theories and forcing the lines to separate. The axis ranges are identical to those of figure 13. Symmetric modes appear as dashed lines, antisymmetric modes as solid lines.

the tension term in (5.17) is generally small, but grows larger near the line $\nu^2 = \zeta$ and causes the shift in modal frequencies evident in figures 12 and 13.

Based on these ideas, we may form a view of how figures 12 and 13 arise. One could imagine trying to attack the problem with *decoupled* theories of extension and of constrained bending. One might use, respectively, membrane shell theory, and the infinite-curvature limit discussed earlier in equation (5.25). Membrane shell theory is the result of neglecting the bending term in (5.17) and dropping the boundary conditions (5.18) and (5.19). For this theory, we find immediately that $\nu^2 = \zeta$. The constrained bending theory, on the other hand, produces frequencies uninfluenced by curvature. Plotting both on a diagram like figures 12 and 13, we obtain figure 15. There are horizontal lines for the 'bending' modes (frequencies for the clamped case have been used), and the rising line $\nu^2 = \zeta$ from the membrane shell theory. This represents a reasonable approximation to what really happens, except near the ringed points where lines corresponding to modes with the same symmetries cross. In those regions there is strong coupling between bending and extension, as just explained, so that the diagram must be modified by the usual phenomenon of repulsion or 'avoided crossing'. The result is a good qualitative match to figure 13, and the same construction using the hinged frequencies gives a similar match to figure 12. We might thus view those figures as showing that all modes except the lowest antisymmetric mode of the flat strip are largely uninfluenced by curvature, but that this lowest mode is influenced so strongly that it is progressively 'rejected' from the system along the line $\nu^2 = \zeta$, coupling to each of the other antisymmetric modes in turn as it passes through the appropriate frequencies.

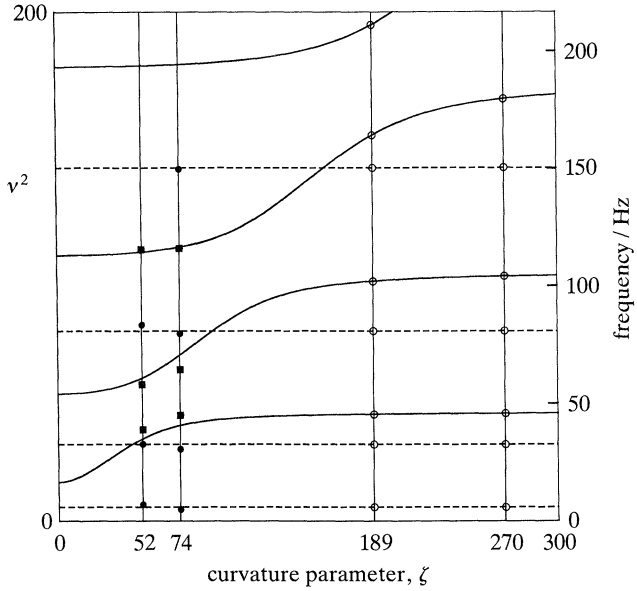

Figure 16. A portion of figure 13, showing the comparison with experimental results. The two vertical lines with open circles show the predictions based on fully clamped ends, while the two lines on the left represent a best fit of the measurements (solid circles and squares for symmetric and antisymmetric mode frequencies respectively) to the theory allowing for finite axial stiffness of the supports.

Table 5. *Measured bending beam frequencies for the two clamped cases*

$\eta = 0.98$		$\eta = 1.4$	
frequency/Hz	symmetry	frequency/Hz	symmetry
6.7	s	4.9	s
32.4	s	30.5	s
39.1	a	45.2	a
58.0	a	65.3	a
83.6	s	80.0	s
115.4	a	116.6	a
		150.8	s

(*c*) *Experimental comparison and model refinement*

We now compare the above theory with the experimental results. In the measurements a steel strip was used, whose physical parameters were all given in §4. Four different S-shaped configurations were studied, with values of η ranging from 0.98 to 2.1. Two of these were achieved by clamping the strip between blocks, the other two were hand-held. For the present purpose, only the two clamped cases are of interest. The length of strip between the clamping blocks, l, was 0.85 m. Table 5 lists the mode frequencies and symmetries found in these two cases. The second case, with $\eta = 1.4$, gave the mode shapes shown in figure 11.

The values of ζ corresponding to these two configurations are respectively 189 and 270. The open circles on the two vertical lines at the right-hand side of figure 16 show what the theory of §5*b* predicts for mode frequencies with these values, assuming clamped boundary conditions. It is immediately apparent that something is seriously

wrong. Without examining the detailed mode frequencies, we see that in both cases the antisymmetric/antisymmetric pair is predicted to lie far too high in the mode sequence. The experimental data show the sequence to begin s/s/a/a followed by alternating symmetric/antisymmetric pairs, for both cases studied. We conclude that, although the qualitative features of the experimental results match those of the theory, the effects of curvature were in fact smaller than predicted.

The most likely explanation lies in the method used to clamp the strip, using wooden blocks. Although the clamps were effective at constraining normal motion and rotation (i.e. $W = W' = 0$), the constraint on stripwise motion (U) could be less effective because thin strips are much stiffer in stretching than in bending, and by comparison the blocks are roughly equally effective in both. It is therefore appropriate to relax the constraint that $U = 0$ and endow the clamps with finite stiffness. The analysis may be extended readily to allow for finite stiffness, both for the clamped case described above and the hinged case, $W = W'' = 0$. The free–free modes and each of the symmetric modes are not changed because they do not involve strip tension; they remain those of a flat strip.

The spring stiffness of the clamps may be modelled by adding a term $\epsilon[U^2(\frac{1}{2}\bar{l}) + U^2(-\frac{1}{2}\bar{l})]$ to the non-dimensional lagrangian

$$\int_{-\frac{1}{2}\bar{l}}^{\frac{1}{2}\bar{l}} \bar{L}\,\mathrm{d}\bar{x}$$

used previously. Here, ϵ is a non-dimensional spring stiffness. This term does not change the equations of motion of the strip nor the end boundary conditions on W, but the end boundary conditions on U are changed to read

$$\tau = \pm\epsilon U(\mp\tfrac{1}{2}\bar{l}) \tag{5.29}$$

to express the effect of the springs. The only effect on the equations of motion and boundary conditions for W is that (5.16) is modified to become

$$\bar{l}\tau = -\frac{1}{1+2/\epsilon\bar{l}}\int_{-\frac{1}{2}\bar{l}}^{\frac{1}{2}\bar{l}} \bar{\kappa}W\,\mathrm{d}\bar{x}, \tag{5.30}$$

i.e. the multiplying constant is changed.

Within the approximations of this analysis, the only result of finite stiffness on ν and W is to multiply the curvature parameter, ζ, by a factor $(1+2/\epsilon\bar{l})^{-\frac{1}{2}}$. This surprisingly simple result indicates that finite stiffness reduces the effective curvature of the strip. As the spring constant $\epsilon \to \infty$ the effective curvature parameter takes on its originally defined value and we recover the theory with fixed U at the ends of the strip. In the opposite limit, $\epsilon \to 0$, the effective curvature parameter drops to zero.

We may thus use figure 16 without alteration to examine results in this modified theory. We have no direct measurement of the likely value of ϵ, so we have attempted to find a good fit of both sets of experimental frequencies with one value of ϵ. The result is seen in the two vertical lines near the left-hand side of the figure. With an assumed value for the factor $(1+2/\epsilon\bar{l})^{-\frac{1}{2}}$ of 0.27, satisfactory agreement with both sets of data is achieved, not only in the sequence of symmetries but also in the detailed frequencies. Measured frequencies of symmetric modes are shown as solid circles, antisymmetric modes as squares.

Most of the divergences of these measured frequencies from the curves can safely be attributed to deviations of the actual experimental conditions from the ideal

conditions assumed by the theory. These details have been discussed in §4. However, there is one feature perhaps worthy of comment. The first two antisymmetric mode frequencies on each line deviate from the theoretical curves in a systematic way. In the light of the discussion at the end of §5*b*, the form of this deviation gives the impression that the coupling between bending and in-surface motions, which is responsible for the anomalous sequence of symmetries, is rather too strong in our theory than in reality. There is no parameter in the theory whose value controls the strength of this coupling, so we have no scope to adjust anything. The effective strength of coupling is built in to our theory from the initial formulation in terms of shallow shell theory, and one would have to look to a more sophisticated formulation to try to resolve this possible anomaly. However, it seems that the present very simple theory captures the essential phenomenon qualitatively correctly, and with reasonable quantitative accuracy.

6. Conclusions

The vibration behaviour of an elastic strip with curvature varying continuously along its length has been studied. It has been shown that when the profile of the strip has an inflection point, as when the strip is bent to an S-shape, then it is possible for certain modes to be confined to the vicinity of the inflection by a process of total internal reflection from points of critical curvature. These modes are then not influenced at all by boundary conditions at the ends of the strip. This accounts for the phenomenon of the 'musical saw', and may also have significance for other problems of shell vibration.

Theoretical modelling has been developed based on an assumption of slowly varying curvature. This analysis revealed the essential nature of the internal reflection process, in terms of the change with curvature of the dispersion characteristics of the strip. From this it appeared that confinement was possible for normal modes based on all the waveguide modes of the strip except the lowest, 'bending-beam', mode. A separate asymptotic analysis of the lowest normal modes in a given series revealed, surprisingly, that the formula for frequencies resulting from the slowly varying theory can be expected to work well down to the very lowest frequencies, even though the mode shapes then bear no resemblance to the slowly varying waves assumed by that theory.

The predictions of the theory were tested by experimental measurements on a steel strip bent into a range of different S-shapes. Frequencies and mode shapes for normal modes based on the second symmetric waveguide branch were measured. Good agreement with the theoretical predictions was shown in all cases.

The bending-beam modes observed in the same experiments have also been investigated. These were found not to follow the usual alternating sequence of symmetry and antisymmetry. It turns out that the symmetric modes are unaffected by curvature, but that with hinged or clamped boundary conditions the antisymmetric modes are influenced strongly by a constraint arising from coupling to in-surface motion, and this accounts for the disturbed symmetry sequence. An assumption of totally clamped boundary conditions did not yield good quantitative agreement with measured frequencies, but satisfactory agreement was obtained when the boundary conditions were relaxed to involve clamping for the transverse motion, but finite spring stiffness for the in-surface motion.

The mode confinement phenomenon studied in this paper is not restricted to

PHILOSOPHICAL TRANSACTIONS OF THE ROYAL SOCIETY A MATHEMATICAL, PHYSICAL & ENGINEERING SCIENCES

problems in which the curvature varies only in one dimension. This one-dimensional problem was studied first, as the simplest exemplar of the effect. However, one can expect to find very similar behaviour in shells whose curvature varies in two dimensions in such a way as to produce a minimum of curvature in some region. An example is the Caribbean steel drum, in which the various tuned notes arise from vibration modes which are confined to different regions within the drum. Each of these tuned regions has low curvature, entirely surrounded by areas of higher curvature. It is possible that analysis similar to that carried out in this paper could be applied to the study of such two-dimensionally curved shells.

Finally, it should be noted that the discussion of confined modes in this paper has not been directed primarily at explaining all details of performance on a musical saw. We have been more concerned with the underlying physics of the confinement process, and we chose the simplest possible system to study this process. In particular, we considered a parallel-sided strip, whereas a normal saw blade has a tapering width. This feature is probably quite important for the saw-player, in attaining a reasonable range of musical notes. There are two obvious mechanisms for varying the pitch of the lowest confined mode of the second symmetric waveguide branch: increasing the severity of curvature, an effect which is included in our analysis, and choosing to place the inflection point at a wider or narrower part of the saw, an effect we have not considered explicitly. However, there is no reason to suspect any subtleties in the physics of this latter effect, the waveguide cut-on frequency simply adjusting to the local width near the inflection point.

The authors are very grateful to Dr B. E. Richardson for the hologram reproduced in figure 4, and to Dr C. Y. Barlow, Mr R. Brand and Mr J. Walden for assistance with the experimental measurements.

References

Abramowitz, M. & Stegun, I. A. 1972 *Handbook of mathematical functions*. Washington, D.C.: Bureau of Standards.

Pippard, A. B. 1983 *The physics of vibration, part 2*. Cambridge University Press.

Rayleigh, Lord 1894 *The theory of sound*. (Reprinted by Dover (New York) 1945.)

Received 4 June 1991; revised 19 September 1991; accepted 25 October 1991

PHILOSOPHICAL TRANSACTIONS OF THE ROYAL SOCIETY A MATHEMATICAL, PHYSICAL & ENGINEERING SCIENCES

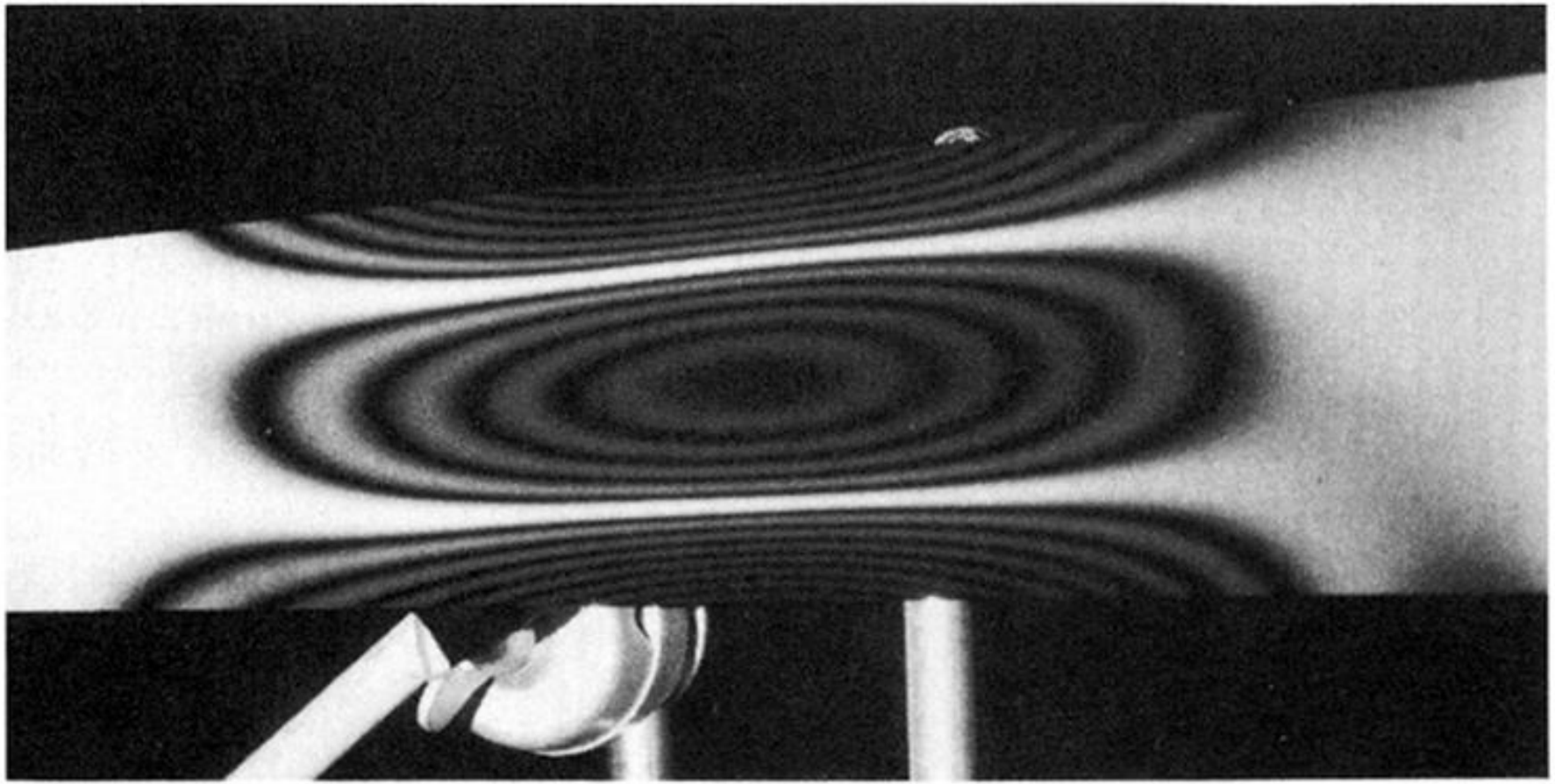

igure 4. Holographic interferogram of the first confined mode on an S-shaped elastic strip, orresponding to the second symmetric waveguide branch. The strip is a different one from that udied experimentally in this paper, but the behaviour is very similar. Photograph kindly rovided by Dr B. E. Richardson.